Jim Starnes' Contributions to Residual Strength Analysis Methods for Metallic Structures

Richard D. Young,[*] Cheryl A. Rose,[*] and Charles E. Harris[†]
NASA Langley Research Center, Hampton, Va 23681-2199

A summary of advances in residual strength analyses methods for metallic structures that were realized under the leadership of Dr. James H. Starnes, Jr., is presented. The majority of research led by Dr. Starnes in this area was conducted in the 1990's under the NASA Airframe Structural Integrity Program (NASIP). Dr. Starnes, respectfully referred to herein as Jim, had a passion for studying complex response phenomena and dedicated a significant amount of research effort toward advancing damage tolerance and residual strength analysis methods for metallic structures. Jim's efforts were focused on understanding damage propagation in built-up fuselage structure with widespread fatigue damage, with the goal of ensuring safety in the aging international commercial transport fleet. Jim's major contributions in this research area were in identifying the effects of combined internal pressure and mechanical loads, and geometric nonlinearity, on the response of built-up structures with damage. Analytical and experimental technical results are presented to demonstrate the breadth and rigor of the research conducted in this technical area. Technical results presented herein are drawn exclusively from papers where Jim was a co-author.

I. Introduction

The present paper summarizes advances in residual strength analyses methods for metallic structures that were realized under the leadership of Dr. James H. Starnes, Jr. Dr. Starnes, respectfully referred to herein as Jim, had a passion for studying complex response phenomena and dedicated a significant amount of research effort toward advancing damage tolerance and residual strength analysis methods for metallic structures. In this research area, Jim's efforts were focused on understanding damage propagation in built-up fuselage structure with widespread fatigue damage, and on understanding the effects of damage on the structural response of built-up fuselage structure, with the goal of ensuring safety in the aging international commercial transport aircraft fleet.

The majority of research led by Jim Starnes in the area of damage tolerance and residual strength analysis of metallic structures was conducted in the 1990's under the NASA Airframe Structural Integrity Program (NASIP). This program, headed by Dr. Charles E. Harris, covered a wide range of topics including fatigue and fracture of materials, nondestructive inspection methods, and residual strength analysis methods for built-up structures with damage. Jim led the structures element of the program, and within this activity Jim supervised, mentored, and collaborated with junior researchers Ms. Vicki O. Britt, and Drs. Richard D. Young and Cheryl A. Rose. Jim also worked closely with Dr. James C. Newman, 'champion' of the critical Crack-Tip-Opening Angle (CTOA) fracture criterion for elasto-plastic fracture, to incorporate the elasto-plastic criterion in residual strength analysis methods, and to help define laboratory scale experiments and critical loading scenarios for validation of the criterion. In addition, Jim supported and collaborated with Dr. Charles Rankin at Lockheed, Palo Alto, to incorporate crack modeling and residual strength analysis methodologies into the STAGS (STructural Analysis of General Shells) general-purpose finite element code.[1]

Jim's approach to research in damage tolerance and residual strength analysis methods for metallic structures was typical of his approach to solving complex problems. The first step in the approach was defining the overall research problem. Several components contributed to the problem definition. First, there was a motivational component, or a driving force for solving the problem. Typically, the driving force was a problem experienced by the aeronautics industry. Jim's connection with industry was invaluable; he had the respect and confidence of manufacturers and operaters, and they often conveyed to him issues or failures that were occuring that they didn't understand. He then relied

---

upon his intuition and extensive expertise in structural mechanics to define preliminary studies to characterize the problem. The preliminary studies were typically tests or simplified analyses of complex built-up configurations, conducted to obtain qualitative information on relevant structural parameters, fundamental structural response characteristics and failure scenarios, and to identify critical loading conditions. Jim would consider results from these studies, and factor in industry input, to formulate the overall problem definition, and then form a vision toward a solution. This vision often consisted of multiple research elements, and the integration of the individual elements. Each research element addressed a critical component of the larger problem, and was defined by breaking the complex response of built-up structure down into contributing factors to be studied separately. Research of each element consisted of detailed numerical and experimental studies of a simplified structural configuration conducted to develop a quantitative understanding of critical response mechanisms identified in the preliminary studies. Each research element provided a stand-alone technical result for a simple application and provided insight into understanding the response characteristics of a more complex configuration. In addition, the individual research elements often resulted in the development of new analysis capabilities that were eventually integrated to develop high-fidelity analysis capabilities for quantitative characterization of the real-world built-up structure.

In the present paper results of research activities in residual strength analysis methods for metallic structures that were conducted in collaboration with Jim are presented following an outline based upon the research approach described above. First, the motivation for the research and the overall problem definition is described. Then results of selected research activities that were defined based upon fuselage structure response characteristics observed in the preliminary studies conducted to define the problem, are presented. The research activities described are presented in order of increasing complexity. First results of a numerical study of nonlinear bulging factors in unstiffened aluminum shells is presented. This study examined the effect of geometric nonlinearity and combined loading conditions on the crack-tip stress intensity factor in an unstiffened shell. The second study extended the previous study's efforts in unstiffened shells to stiffened structure, including detailed modeling of stringer and fastener parameters. The final section presents a summary of research activities that were specifically focused on the development and validation of a high-fidelity residual strength analysis methodology for aircraft aluminum fuselage structures with cracks and subjected to combined internal pressure and mechanical loads. The method accounts for all of the complexities present in a fuselage shell structural response that must be represented to predict accurately fuselage structure residual strength. The methodology is based upon the critical crack-tip-opening-angle (CTOA) elastic-plastic fracture criterion to represent stable crack growth and fracture in ductile materials, and a geometric and material nonlinear shell analysis code to perform the structural analysis.

II.   Problem Definition

Commercial transport are designed with a damage tolerant design philosophy that requires the aircraft to maintain adequate structural integrity in the presence of discrete source damage or fatigue cracks. As economic and market conditions encourage the use of commercial airplanes beyond their original design service life, it is important to be able to predict the fatigue life and residual strength of fuselage structures with cracks. Widespread fatigue damage (WFD) is a significant concern for the aging aircraft fleet because the residual strength of structure with a long crack might be significantly reduced by the existence of adjacent smaller cracks.[2] The accident of the Aloha aircraft, shown in Fig. 1, made aging aircraft a national priority. The Aloha aircraft accident is an example of widespread fatigue damage, where several short fatigue cracks along a fuselage lap joint linked together and unzipped an 18-foot-long section of the crown of the fuselage. One flight attendant was killed, but, amazingly, the pilot was able to land the aircraft. Another example demonstrating the threat to the structural integrity of aging aircraft is shown in Fig. 2. The aircraft shown in this figure was damaged when a fatigue crack from a manufacturing flaw caused engine failure during take-off. Uncontained engine debris from the engine penetrated the fuselage, killing two passengers and significantly compromising the structure.

The Aloha aircraft resulted in the launching of NASA and FAA initiatives in aging aircraft. One of the objectives of the NASA Airframe Structural Integrity Program (NASIP) was to develop an analysis methodology for predicting failure of damaged fuselage structures in the presence of widespread fatigue damage. The structural response of a stiffened fuselage with long cracks, such as mid-bay cracks or splice joint cracks after MSD link-up, is extremely complex, and is influenced by local stress and displacement gradients near the crack, and by the internal load distribution in the shell. This complex response needed to be understood in order to develop a residual strength analysis methodology for fuselage structures with cracks.

Figure 1. Wide-spread fatigue damage causes in-flight fuselage crown panel separation. Aloha Airlines Boeing 737, April 28, 1988.
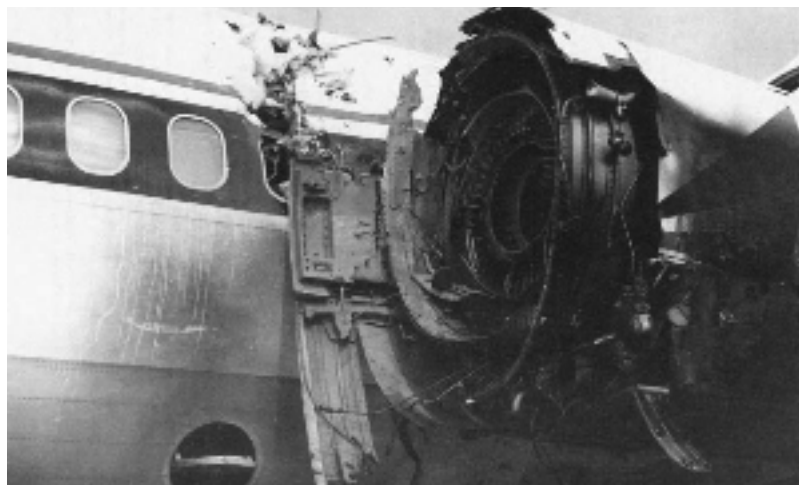

Figure 2. Engine failure during take-off with uncontained debris penetrating fuselage. Delta Airlines, MD-88, July 6, 1996.

Early work conducted in the NASIP program and led by Jim Starnes focused on developing an understanding of the effects of combined loads and geometric nonlinearity on the response of complex built-up fuselage structure.[3-5] Analytical studies of the nonlinear response of stiffened shells with long cracks were conducted using relatively coarse models of a stiffened shell to obtain qualitative information on the effects of crack location, crack orientation, and various combinations of internal pressure and mechanical loads on the response characteristics. Results from a typical early study are shown in Fig. 3. In this case, an analytical study was conducted for a full-barrel fuselage with a longitudinal crack in the crown, and subjected to internal pressure loading, and internal pressure plus up-bending and down-bending moments. The crack edges are loaded in axial compression when an up-bending moment is applied and in axial tension when a down-bending moment is applied. The results shown in Fig. 3 indicate that the local crack deformations are symmetric, so fracture is governed by the symmetric crack-opening stress-intensity factor. In addition, the results indicate that the symmetric crack-opening stress-intensity factor is the largest for the up-bending moment case, where there is local axial compression along the crack edges, and is the smallest for the down-bending moment case. These results demonstrate sensitivity to combined loads and also represent a geometrically nonlinear response, as linear analyses do not indicate such a combined load effect.

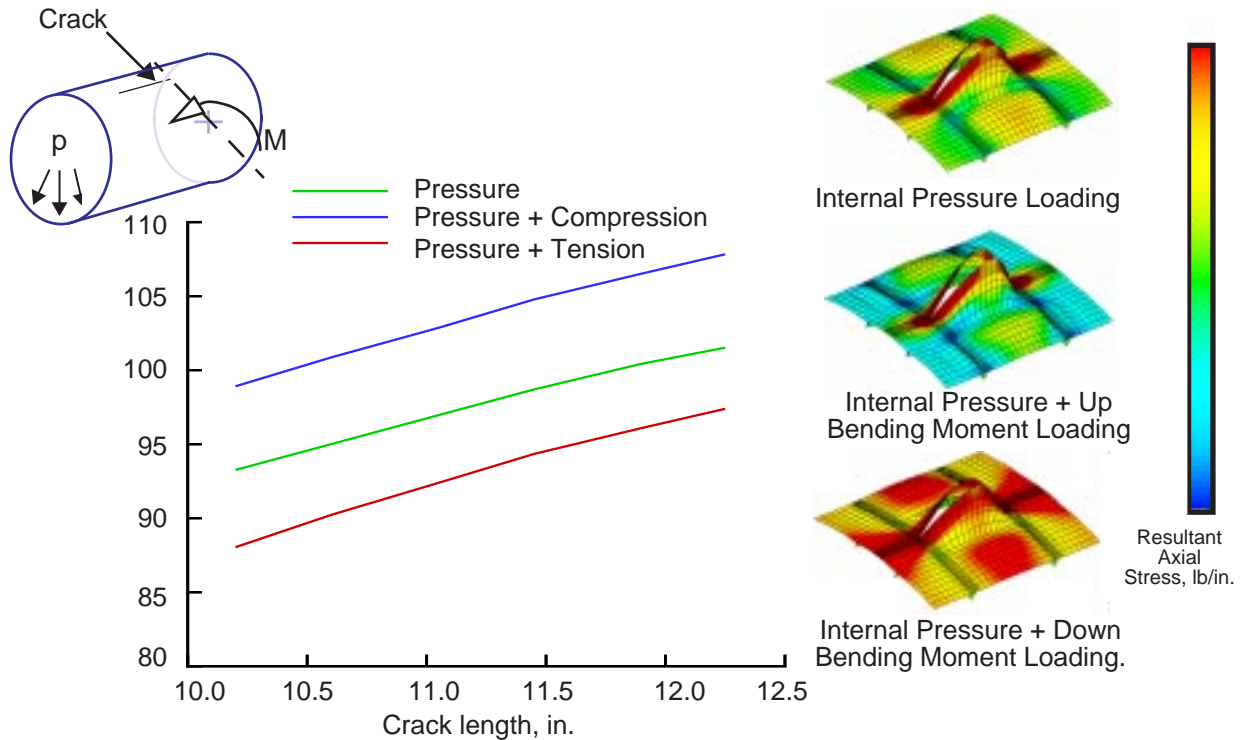American Institute of Aeronautics and Astronautics

Figure 3. Crack-opening stress-intensity factor for a longitudinal crack in a fuselage shell subjected to internal pressure loading, and internal pressure loading plus an up-bending and a down-bending moment.

Additional preliminary studies were conducted to determine the effect of crack location within the fuselage structure, and the effect of shear and torsion fuselage loadings on the local crack deformations and stress-intensity factors. Results from these studies indicated that torsion loads can cause an increase in the crack-shearing stress-intensity associated with a crack. Results also showed that the crack-growth trajectory can be influenced by the crack location and the loading condition. A typical result from a study of the effects of loading condition and crack location on crack-growth trajectories is shown in Fig. 4. Crack growth trajectories are shown in Fig. 4 for three longitudinal crack locations and loading conditions. The crack is either located midway between two stringers or 1.2 inches from a stringer. The crack-growth trajectory for a crack located midway between two stringers in a panel that is subjected to internal pressure, up-bending and vertical shear loads is shown in Fig. 4a. The crack-growth trajectory for this case is self-similar due to the symmetry of the loading and the geometry. The crack-growth trajectory for a crack located 1.2 in. from a stringer in a panel that is subjected to internal pressure, up-bending and vertical shear loads is shown in Fig. 4b. In this case the crack-growth trajectory is non-self-similar due to the nonsymmetry of the geometry. The crack-growth trajectory for a crack that is located midway between two stringers in a panel that is subjected to internal pressure and torsion loads is shown in Fig. 4c. The crack-growth trajectory for this case is non-self-similar due to the non-symmetry of the loading condition.

These and additional preliminary results demonstrated important aspects of the response of a long crack in a stiffened fuselage shell and several general conclusions were drawn from these initial studies. First, long cracks can change the internal load distribution in a stiffened shell. Second, the pressure only loading case, which is typically used as the critical design condition in practice, can result in unconservative predictions for the fuselage shell residual strength. Therefore, the effects of combined loads must be considered. Third, the local shell response is geometrically nonlinear, as evidenced by the effect of combined loads on the crack-tip stress-intensity. Local displacements near a crack can be large compared to the fuselage thickness, and these displacements can couple with internal stresses resultants in the shell to amplify magnitudes of the local stresses and displacements near the crack. Fourth, the crack behavior is strongly influenced by structural stiffening elements. Furthermore, fracture of fuselage structues made from ductile aluminum alloys exhibit a large degree of plasticity near the crack tip. Thus, a fracture criterion that accounts for elastic-plastic material nonlinearity would be also be required. All of these complexities are present in a
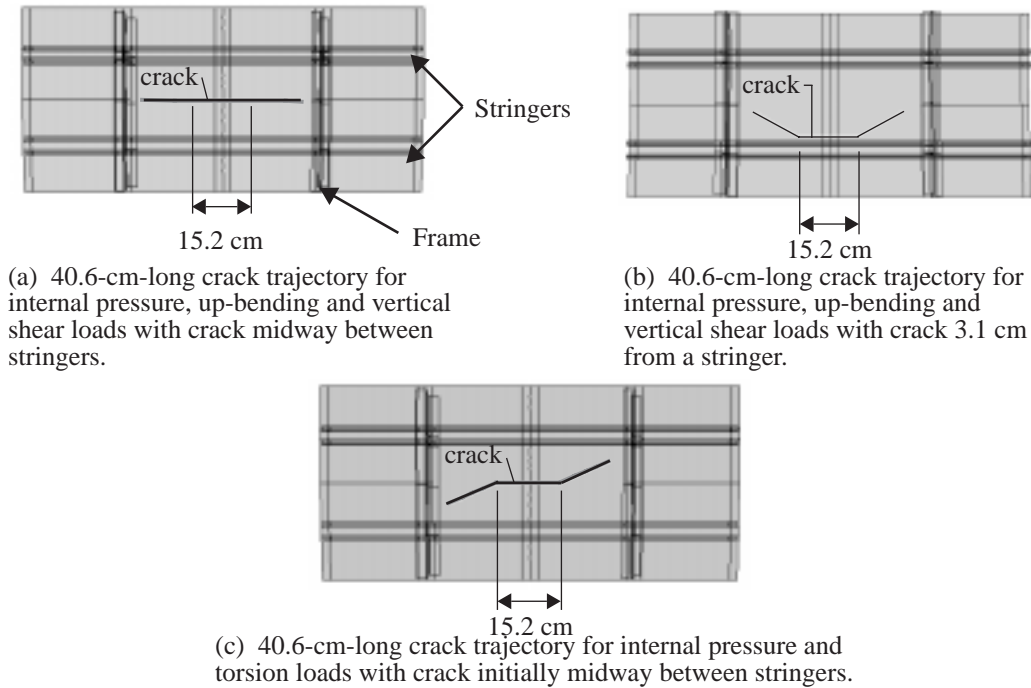
American Institute of Aeronautics and Astronautics

(a) 40.6-cm-long crack trajectory for internal pressure, up-bending and vertical shear loads with crack midway between stringers.

(b) 40.6-cm-long crack trajectory for internal pressure, up-bending and vertical shear loads with crack 3.1 cm from a stringer.

(c) 40.6-cm-long crack trajectory for internal pressure and torsion loads with crack initially midway between stringers.

Figure 4. Effect of fuselage loading condition and crack location on crack growth trajectories.

fuselage shell structure with damage and must be addressed in residual-strength analysis methods for fuselage structure.

Jim Starnes integrated information from these preliminary analyses, from industry experience, and from his own expertise to formulate a general problem statement for research in residual strength analyses methods for metallic structures with damage. The goal of this research was to develop, and verify by experiment, a residual strength analysis methodology for fuselage structures that incorporates the inherent response characteristics described above. Jim was a strong advocate for high-fidelity analysis methods, believing that eliminating empiricism whenever possible would increase general understanding of relevant parameters and reduce the chance for applying empirical factors inappropriately.

Jim's vision for addressing the general research problem described above consisted of separating the complex general problem into several research elements, each designed to consider part of the more-general problem. In the next two sections of this paper, results from two such research elements are summarized. These results are drawn from references that contain complete details of each research element.

III. Nonlinear Bulging Factors

A study on nonlinear bulging factors for pressurize fuselage shells is described in Ref. 6. The objective of this study was to establish a solid understanding of the effects of curvature, combined loads, and geometric nonlinearity on linear elastic fracture parameters for unstiffened shell structures. The study was motivated by the traditional approach to residual strength analyses and damage tolerant design that relied primarily on geometrically linear analyses and fracture analyses based on linear elastic fracture mechanics. Linear elastic fracture mechanics suggests that the crack-tip stress intensity factor is an indicator of the likelihood of fracture. The conventional engineering approach used in design practice was to predict the crack-tip stress intensity factors for a crack in a fuselage shell by applying a so-called "bulging factor," in combination with additional design factors that account for stiffener elements, to the stress intensity factor for a flat plate subjected to similar loading conditions. Results of the preliminary studies described previously suggested that residual strength predictions based on the pressure-only loading case may be unconservative if the loading has axial compression.

The bulging factor accounts for the fundamental difference in behavior of a crack in a curved shell compared to the behavior of a crack in a flat plate. In a cracked shell, the local region around the crack deforms out-of-plane as a

result of the curvature induced coupling between the membrane and bending displacements, and the internal pressure, where, in a plate, the crack deforms in plane. These out-of-plane displacements in the neighborhood of a crack in a shell increase the crack opening and crack-tip stress intensity compared to those of a cracked plate with the same crack geometry. The bulging factor, β, amplifies the flat-plate stress intensity factor and is defined as the ratio of the stress intensity factor K_s in a shell with a crack, to the stress intensity factor K_p in a flat plate of the same material, thickness, crack length, and in-plane remote stress, σ, acting perpendicular to the crack line:

$$\beta = \frac{K_s}{K_p} \tag{1}$$

Many studies have been conducted to characterize bulging cracks, and both analytical[7-14] and empirical formulas[15-20] for the bulging factor have been developed. Analytical expressions for the bulging factor in shells were developed using formulations based on linear shallow shell theory. These analytical expressions depend on the shell curvature parameter, λ, where, for an isotropic shell, λ is defined as:

$$\lambda = \frac{a}{\sqrt{Rt}} \sqrt[4]{12(1 - v^2)} \tag{2}$$

and:

$$v = Poisson's\ ratio$$
$$a = half\ crack\ length$$
$$R = radius\ of\ the\ shell$$
$$t = thickness\ of\ the\ shell$$

The analytical bulging factors based on linear shallow shell theory tend to overestimate the physical bulging effect, unless the cracks are very short, or the applied load is very small, so that geometric nonlinear effects are not significant. For longer cracks or higher loads, tensile membrane stresses develop along the crack edges as the crack bulges. These tensile stresses increase the resistance to additional crack bulging and crack opening, and result in a reduction in the bulging factor.[21-22] Empirical formulas, which attempt to account for the nonlinear character of the bulging response, were also developed for determining bulging factors in shells with longitudinal cracks.[17-20] These empirical formulas were developed for specific materials, geometries and loading conditions, and thus, the formulas are valid for limited applications.

A more general investigation of the geometrically nonlinear response of pressurized cylindrical shells with longitudinal cracks was conducted by Budiman and Lagace.[23,24] Budiman and Lagace, under a grant sponsored by Jim Starnes, demonstrated that the nonlinear response of cylindrical shells with longitudinal cracks, subjected to internal pressure loading, can be characterized by two nondimensional parameters: the shell curvature parameter, λ, as defined in Eq. (2); and a loading parameter, η, which depends on the applied internal pressure, material properties, and shell geometry. Research conducted by Young, Rose, and Starnes[25,26] extended the study conducted by Budiman and Lagace by investigating the geometrically nonlinear response of pressurized cylindrical shells with long longitudinal and circumferential cracks and the effects of combined loads on the bulging factor. A comprehensive numerical parametric study of the geometrically nonlinear response of unstiffened aluminum shells with centrally located longitudinal and circumferential cracks subjected to combined internal pressure and mechanical loads was conducted using the STAGS nonlinear finite element analysis code. Major results of the study were contour plots for the bulging factor, β, and empirical expressions for estimating the bulging factor for longitudinal and circumferential cracks in both the linear and nonlinear region of the response. Contour plots of the bulging factor are presented in terms of three nondimensional parameters: the curvature parameter λ, a pressure loading parameter, η, defined as:

$$\eta = \sqrt{\frac{\sigma_y R}{E\ t}} (\sqrt[4]{12(1 - v^2)}) \tag{3}$$

where σ_y is the farfield circumferential stress, and the biaxial loading parameter,

$$\chi = \sigma_x / \sigma_y. \tag{4}$$

Longitudinal crack

Typical results obtained in the study for the bulging factor for a longitudinal crack in a cylindrical shell, β^L, as a function of the shell curvature parameter, λ, and the pressure loading parameter, η, are presented as contour plots in Fig. 5. Bulging factors for $\chi = 0.0$, 0.5, 1.5, and 6.0, are shown in Fig. 5a, 5b, 5c, and 5d, respectively. The solid lines in the figure are contour lines, or lines through points with a common value of the bulging factor. There are some
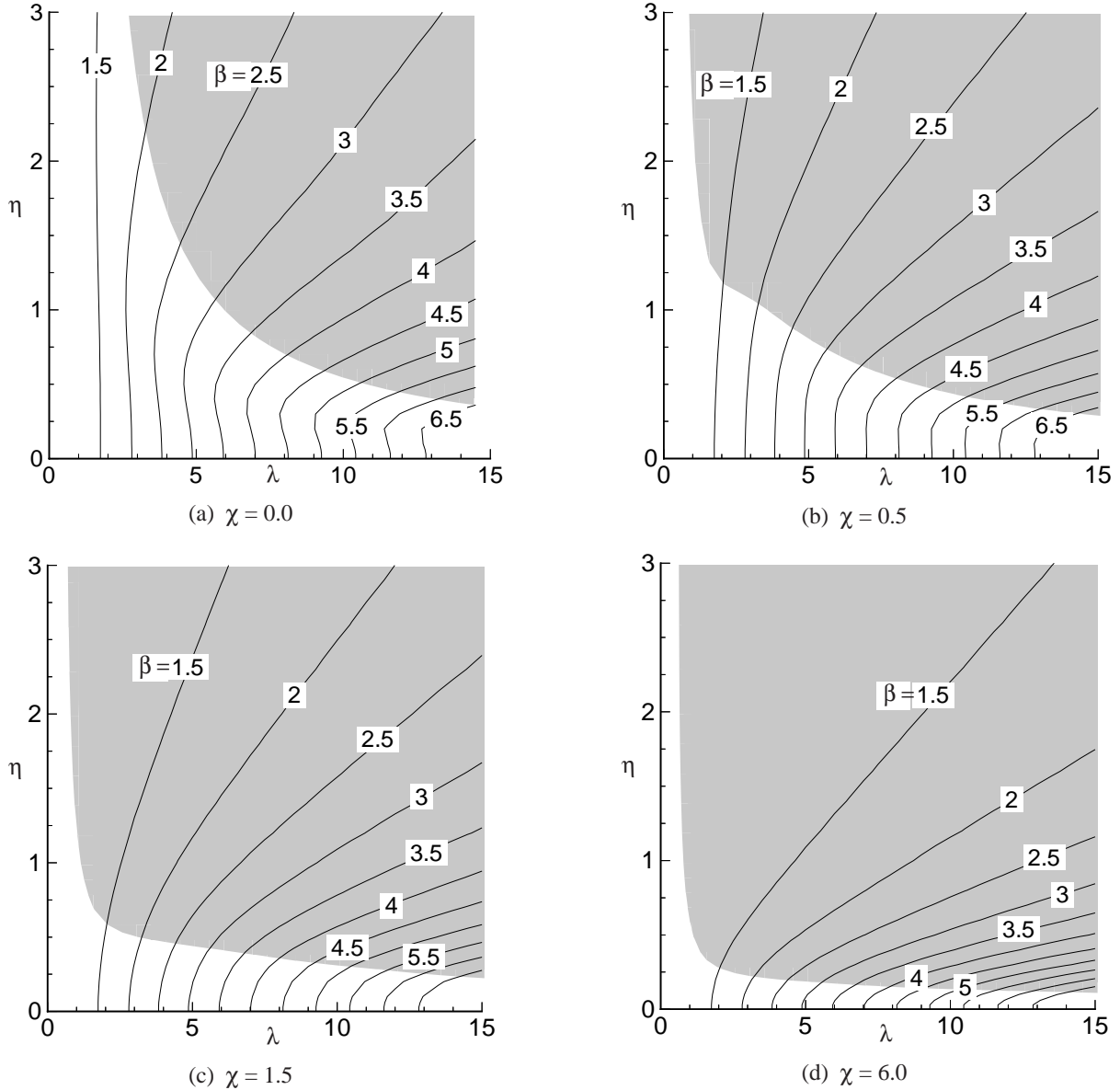
(a) $\chi = 0.0$

(b) $\chi = 0.5$

(c) $\chi = 1.5$

(d) $\chi = 6.0$

Figure 5. Contour plot of the bulging factor for a longitudinal crack, β^L, from STAGS analyses, and the linear (unshaded) region of the bulging factor response, as a function of the shell curvature parameter, λ, and the pressure loading parameter, η, for several values of the biaxial loading parameter, χ.

general trends indicated by the contour plots. For a given value of χ, the bulging factors monotonically increase with increasing values of λ, and generally decrease with increasing values of η. In each contour plot, the bulging factor for very small values of η, i.e., for locations near the λ-axis, corresponds to the linear bulging factor, β^L_{lin} as reported by Erdogan and Kibler[12], and does not vary with changes in χ. For small values of η, the contour lines are nearly perpendicular to the λ-axis, indicating that the bulging factor for small values of η is primarily a function of λ only and can be approximated by β^L_{lin}. The unshaded areas of the contour plots in Fig. 5 indicate the linear region of the response where the difference between β^L and β^L_{lin} is less than 10%. For higher values of η, the bending deformations become sufficiently large and cause nonlinear membrane stiffening. The bulging factors decrease with increasing η, and the contour lines bend to the right and asymptotically approach lines which extend radially from the origin. The shaded areas of the contour plots in Fig. 5 indicate the nonlinear region of the response where the difference between β^L and β^L_{lin} is greater than 10%. The largest differences between β^L and β^L_{lin} occur when λ and η are both large, where β^L_{lin} overpredicts β^L by 45% when $\chi = 0$, and by 400% when $\chi = 6$. Comparison of the contour plots for different values of χ indicates that increasing the biaxial loading parameter promotes tensile membrane behavior, causing

the contour lines to bend to the right at lower values of η, thus reducing the size of the linear response region. A simple expression for representing the bulging factor behavior shown in Fig. 5, that can be easily used in a design environment, is obtained by characterizing the linear and nonlinear regions of the response separately.

The linear region of the response is accurately described by the linear bulging factor for a longitudinal crack, β_{lin}^L. A simple expression for the linear bulging factor is obtained by examining the behavior of the numerical data and determining that the data can be approximated closely by the function

$$\beta_{lin}^L = \sqrt{1 + (0.5)\lambda^{1.725}} \qquad (5)$$

An expression for estimating the bulging factor in the nonlinear region of the response, β_{nl}^L, is obtained by utilizing the fact that the contour lines of the bulging factor asymptotically approach radial lines through the origin. For a given value of χ, the value of the bulging factor can be uniquely related to the slope of the radial line, i.e., λ/η, which is approached asymptotically by a contour line. To obtain an expression which relates the nonlinear bulging factor to the ratio λ/η and the biaxial loading ratio, χ, the relationship between the nonlinear bulging factor and the ratio λ/η is first established for each value of χ. Then, the variation in this relationship is described as a function of χ. By numerical processing of the data represented in Fig. 5, it was determined that β_{nl}^L can be closely approximated by the equation

$$\beta_{nl}^L = \sqrt{1 + [c_1(\chi)][\lambda/\eta]^{c_2(\chi)}} \qquad (6)$$

where the coefficients $c_1(\chi)$ and $c_2(\chi)$ are given by

$$c_1(\chi) = 0.15 + 1.75e^{-0.8\chi}, \text{ and} \qquad (7)$$

$$c_2(\chi) = 1.4 - 0.52e^{-0.43\chi} \qquad (8)$$

By using Eqs. (7) and (8) with Eq. (6), the nonlinear bulging factor for a longitudinal crack in a cylindrical shell, β_{nl}^L, is expressed in terms of the shell curvature parameter, the pressure loading parameter, and the biaxial loading parameter. The expression for β_{nl}^L in Eq. (6) will overpredict the bulging factor in the linear region of the response, while the expression for β_{lin}^L in Eq. (5) will overpredict the bulging factor in the nonlinear region of the response. The bulging factor over the entire linear and nonlinear regions of the response, for any value of λ, η and χ, is approximated by taking the minimum of the linear bulging factor estimated by Eq. (5), and the nonlinear bulging factor, estimated by Eq. (6).

$$\beta_{approx}^L = \min(\beta_{lin}^L, \beta_{nl}^L) \qquad (9)$$

The accuracy of Eq. (9) in representing the bulging factors from the STAGS analyses is demonstrated by the contour plots of the bulging factors for $\chi = 0.0$ and 6.0 shown in Fig. 6a and 6b, respectively. In Fig. 6, the bulging factors from the STAGS analyses are shown as solid lines, and the estimates from Eq. (9) are shown as dashed lines. The largest discrepancies between Eq. (9) and the STAGS analyses occur in the transition region between the linear and the nonlinear regions of the response. For $\chi = 0$, the discrepancies are less than 10% over the entire area. For $\chi = 6$, the shaded area in the contour plot indicates the region where the discrepancies are greater than 10%. The shaded area is small, and the worst case situation for Eq. (9) overpredicts the bulging factor by 22%.

Circumferential Crack

Results obtained for a circumferential crack demonstrated that the bulging factor for cylindrical shells with circumferential cracks, β^C, has a mild dependence on the biaxial loading parameter. The bulging factors for $\chi = 0.5$ are a good estimate for $0.25 < \chi < 6$, and the largest discrepancies are conservative. Thus, the circumferential bulging factor will be characterized for $\chi = 0.5$. The bulging factor results from the STAGS analyses of cylindrical shells with circumferential cracks, β^C, are presented as a function of the shell curvature parameter, λ, and the pressure loading parameter, η, in Fig. 7. The solid lines in the figure are contour lines, or lines through points with a common value of the bulging factor. The results in the contour plot indicate that the bulging factors monotonically increase with increasing values of λ, and monotonically decrease with increasing values of η. This behavior is consistent with the results shown in Fig. 5. The contour plot of the bulging factors for the circumferential crack with $\chi = 0.5$ in Fig. 7 is similar to the contour plot of the bulging factors for the longitudinal crack with $\chi = 0.5$ shown previously in Fig. 5(b). The primary differences between the bulging factor contour plots for the two crack orientations are that the bulging factor for the circumferential crack is smaller in amplitude, and the contour lines are concentrated nearer to the abscissa of the plot. The contour lines are perpendicular to the λ-axis for very small loads, but the contours bend to the right almost
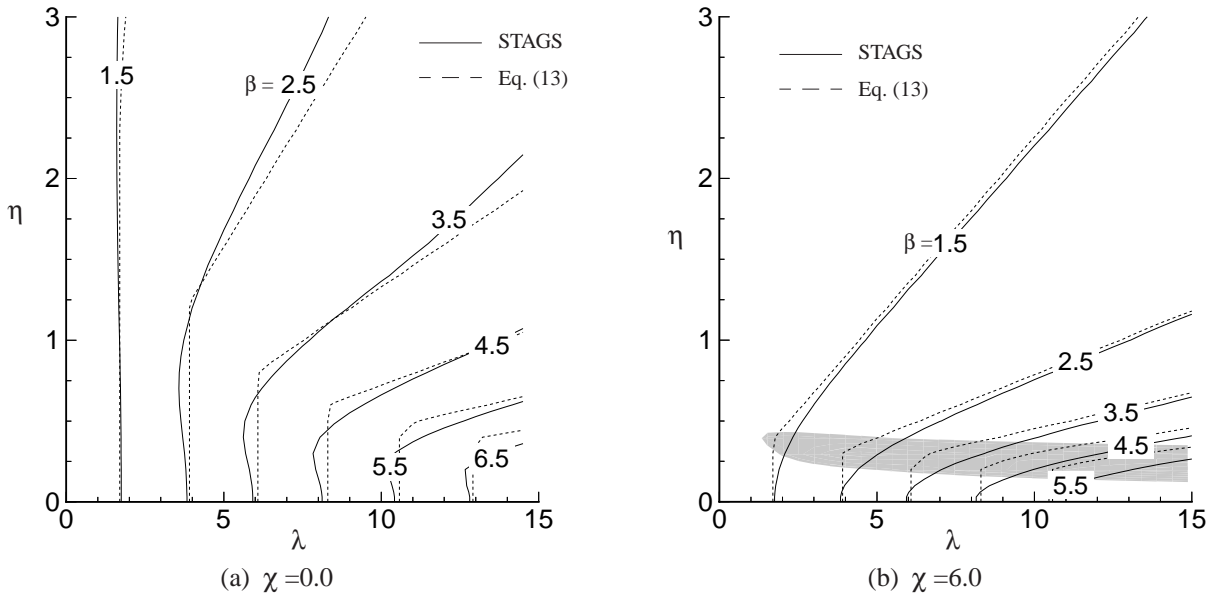
Figure 6. Contour plot showing the bulging factors for a longitudinal crack, β^L, as computed using STAGS and approximated by Eq. (13), as a function of the shell curvature parameter, λ, and the loading parameter, η.

immediately as η is increased, and asymptotically approach lines which extend radially from the origin. The shaded area of the contour plot in Fig. 7 signifies the nonlinear region of the response where the difference between β^C and β_{lin}^C is greater than 10%. This shaded region is closer to the λ-axis than it was for the longitudinal crack with $\chi = 0.5$, indicating that the transition from the linear bending response to the nonlinear membrane response occurs at smaller values of load for a shell with a circumferential crack than for a shell with a longitudinal crack. The largest differences between β^C and β_{lin}^C occur when λ and η are both large, which results in β_{lin}^C overpredicting β^C by 100%.
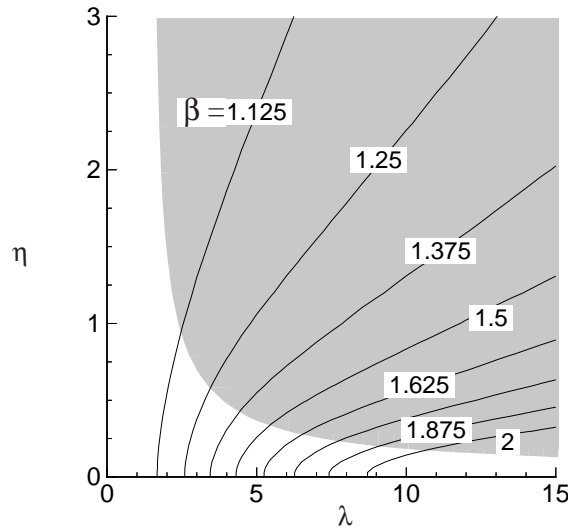

Figure 7. Contour plot of the bulging factor for a circumferential crack, β^C, from STAGS analyses, and the linear (unshaded) region of the bulging factor response, as a function of the shell curvature parameter, λ, and the pressure loading parameter, η.

By applying numerical procedures similar to those applied for the longitudinal crack case, simple expressions that can be easily used in a design environment were generated for a circumferential crack case. The bulging factor for a circumferential crack over the entire linear and nonlinear regions of the response, for any value of λ, η and χ, can be approximated by the expression:

$$\beta_{approx}^C = \min(\beta_{lin}^C, \ \beta_{nl}^C) \tag{10}$$

where

$$(\beta_{lin}^C)^2 = 0.955 + 0.110\lambda + 0.0637\lambda^2 - 00534\lambda^3 + 0.000144\lambda^4 \tag{11}$$

and

$$(\beta_{nl}^C)^2 = 1.05 + 0.122\left(\frac{\lambda}{\eta}\right) - 0.00161\left(\frac{\lambda}{\eta}\right)^2 + 9.27E\text{-}6\left(\frac{\lambda}{\eta}\right)^3 \tag{12}$$

The bulging factors obtained by applying Eq. (10) are compared to the bulging factors from the STAGS analyses in Fig. 8. The bulging factors from the STAGS analyses are shown in Fig. 8 as solid lines, and the estimates from Eq. (10) are shown as dashed lines. The largest discrepancies between Eq. (10) and the STAGS analyses occur in the transition region between the linear and the nonlinear regions of the response. The worst case situation for Eq. (10) overpredicts the bulging factor by 9%.

Summary Remarks

The results presented in this study demonstrated the ranges of the shell curvature and loading parameters for which the effects of geometric nonlinearity are significant, and showed the effect of biaxial loads on the value of the bulging factor. Simple empirical expressions for the bulging factor, derived from the numerical results, were shown to predict accurately the nonlinear response of shells with longitudinal and circumferential cracks. The primary outcome of this research was accurate nondimensional representation of a complex nonlinear response phenomena, that accounts for combined load effects, and presents a direct improvement to current design methodology for damage tolerance of curved shell structures. The results illustrated that for longitudinal and circumferential cracks, the linear bulging factor is generally overconservative, and using the linear factor may result in designs that are significantly overweight. For circumferential cracks, the bulging factor is insensitive to biaxial loads. For longitudinal cracks, the nonlinear bulging factor is a function of biaxial loading, and designing with the nonlinear result for the pressure-only case is unconservative if the actual loading has axial compression, i.e., $\chi < 0.5$.
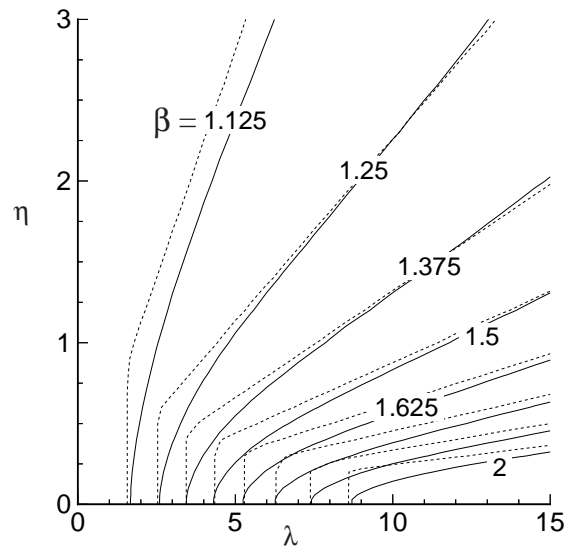

Figure 8. Contour plot showing the bulging factors for a circumferential crack from the STAGS analysis, and from Eq. (16), as a function of the shell curvature parameter, λ, and the pressure loading parameter, η.

IV. Skin, Stringer, and Fastener Loads in Buckled Fuselage Panels

The study described in Ref. 27 extended previous efforts in modeling and understanding the response of unstiffened shells subjected to internal pressure and mechanical loads to more complex built-up structure representative of fuselage structure. Typical metallic fuselage structure consists of built-up stiffened panels with a thin skin attached to longitudinal stringers and circumferential frames. To maximize structural efficiency, fuselage shells are usually designed to allow the fuselage skin to buckle in compression and shear at a load level that is below the design limit load condition for the shell. Thus, it is assumed that cracks may exist in the structure during the service life of the aircraft, and that loading conditions could occur that would cause the fuselage skin with cracks to buckle.

Skin buckling causes nonlinear deformations and changes in the stress distribution in the skin, the internal structure, and the fasteners connecting the skin and the internal structure. Failure initiation and propagation in the built-up structure may involve crack initiation in the skin or stiffening elements, or fatigue or strength failure of the fastener elements connecting the skin to the stiffening elements. The structural integrity of a built-up structure subjected to combinations of internal pressure and mechanical flight loads can be studied analytically with a nonlinear structural analysis capability, but a high-fidelity modeling and analysis methodology must be applied to obtain accurate predictions of the state of stress in each component of the structure. Most residual-strength analysis studies reported in the literature for fuselage shells with cracks[7,11,12,18,19,21-24] have been limited to internal pressure loads only, where the shell is in biaxial tension. The results of analytical studies of the nonlinear response of unstiffened aluminum shells with longitudinal cracks and subjected to internal pressure and axial compression loads[6,17,28-29] have indicated that the crack-growth characteristics of longitudinal cracks are influenced by the biaxial-loading ratio, χ, defined as the ratio of the longitudinal stress resultant to the circumferential stress resultant. The influence of biaxial loading on cracked stiffened panels was reported in Refs. 30 and 4, but skin buckling was not considered in either reference. Rose, Young and Starnes[28] studied the effect of initial cracks on the nonlinear response of a cylindrical shell and found that the buckling load can be significantly reduced by the presence of a crack, and that the buckling load decreases as the crack length increases for a given pressure load. In addition, results of a fatigue test of an A300B fuselage[31] indicated that compressive stress directioned parallel to a crack may increase the stress intensity factor by 40%.

A numerical study was conducted to assess the effect of skin buckling on the internal load distribution in a pristine stiffened fuselage panel, and in a stiffened fuselage panel with longitudinal cracks. In addition, the impact of changes in the internal loads on the fatigue life and the residual strength of a fuselage panel were assessed. Geometrically nonlinear response was considered, and the assessment was simplified by considering linear-elastic material behavior and examining linear-elastic fracture parameters to provide a qualitative measure of the effect of skin buckling on residual strength and life. The STAGS finite element code, which has special features for modeling fastener elements, contact between built-up components, and cracks in shell structures, was used to conduct the analyses.[1] Stress intensity factors for symmetric and anti-symmetric membrane (K_I, K_{II}) and bending (k_1,k_2) modes can be computed within STAGS.[32-33] The total stress intensity factor K_T is calculated from the total strain-energy-release rate, G:

$$K_T = \sqrt{EG} \tag{13}$$

The structural configuration considered in this study is shown in Fig. 9, and is a generic narrow-body fuselage panel. It is constructed entirely of 2024-T3 aluminum alloy, with a 74.-in. skin radius, a 0.040-in. skin thickness, Z-stringers with an 8.-in spacing, and Z-frames with a 20.-in. spacing. A finite element model of the stiffened fuselage panel with two frame-to-frame longitudinal skin bays and five circumferential stringer bays is shown in Fig. 9. The origin of the (x,y) coordinate system shown in Fig. 9 is located on the center stringer, and midway between the frames. The model was defined to include one half of a skin-bay beyond the last stiffening member on each edge of the panel. The circumferential edges of the skin and frames have symmetry boundary conditions. The longitudinal edges of the panel have the rotational constraints of a line of symmetry and multi-point constraints to enforce a uniform longitudinal edge displacement. The Young's modulus, E, for the aluminum alloy is equal to 10.5 msi and Poisson's ratio, v, is equal to 0.33.

The loading condition for the fuselage panel consists of an applied internal pressure, p (which generates a circumferential stress resultant reaction, N_y), and an axial stress resultant, N_x, which is the sum of the bulkhead pressure load, and an applied mechanical load. The stress resultants, N_x and N_y, represent the average load in pounds per inch along the longitudinal and circumferential edges of the panel, respectively. A biaxial loading ratio, χ, is defined as the ratio of the axial load to the circumferential load, $\chi = N_x/N_y$. A biaxial loading ratio $\chi = 0.5$ corresponds to the
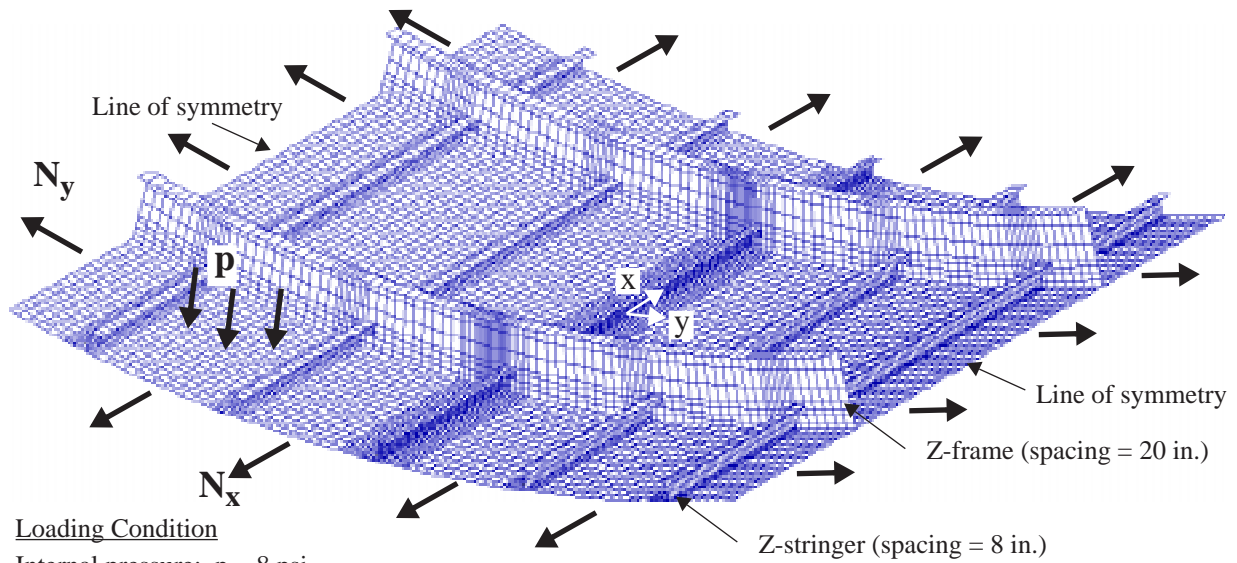
Loading Condition
Internal pressure: p = 8 psi
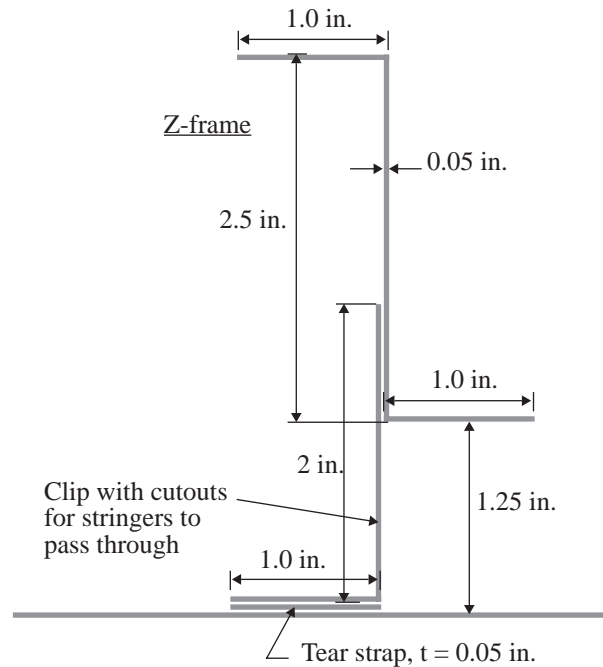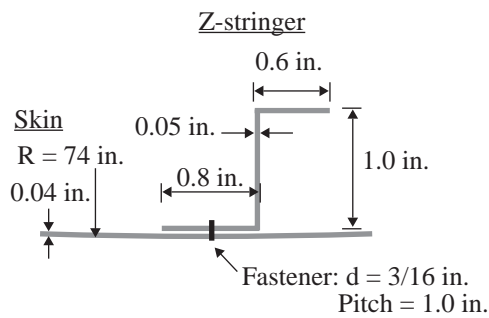Axial load: $N_x = \chi N_y$ (χ = -1.2 to +2)

Figure 9. Geometry and finite element model of stiffened fuselage shell.

internal-pressure-only loading condition. The maximum compression load considered corresponded to a biaxial load-ing ratio $\chi = -1.2$, which was two times the axial compressive load required to buckle the skin of the fuselage panel.

Pristine Panel

Nonlinear analyses were conducted for the fuselage panel with no damage. Solutions were obtained for an in-ternal pressure load of 8 psi, and a range of axial loading values corresponding to biaxial loading ratio values χ = 2.0 to -1.2. Contour plots of the fuselage-skin radial displacement for χ = 0.5 and -1.0 are shown in Fig. 10. The case with χ = 0.5 corresponds to the bulkhead tension load for a nominal pressure load only. The radial displacement result for χ = 0.5, shown in Fig. 10a, shows that the internal pressure on the skin deforms the skin radially outward, and the displacements are smaller where the skin is attached to the stiffening structure. The circumferential stiffness of the
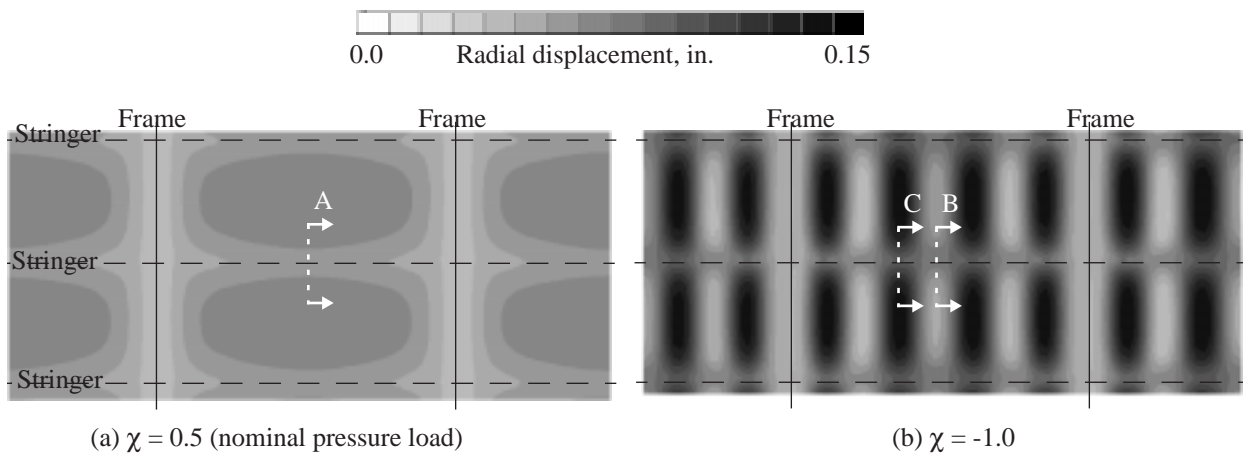
0.0   Radial displacement, in.   0.15

(a) χ = 0.5 (nominal pressure load)   (b) χ = -1.0

Figure 10. Fuselage-skin radial displacement for biaxial loading ratio values of χ = 0.5, and -1.0.

frames strongly resists the radial deformation, thus the skin's radial displacement is the smallest near the frames. The stringers resist radial deformation because they are attached to the frames. The stringers provide some radial support to the skin through the bending stiffness of the stringers. The stringers bend along their length and deflect outward more than the frames, and the skin on each side of the stringer deflects outward more than the stringer. The skin radial displacement for χ = -1.0, shown in Fig. 10b, displays a fully-developed buckled skin pattern that is symmetric with respect to each stringer and each frame. The symmetry in the response is attributed to the strong influence of the bending boundary layer on each side of the frames and the presence of the internal pressure load. Changes in the structural configuration would likely influence the deformation shape and symmetry of the response.

Panel cross sections 'A', 'B' and 'C' are identified in Fig. 10. For each cross section, the deformed shape of the skin-stringer attachment area is shown amplified by a factor of 10 in Fig. 11. For the case with nominal pressure load, χ = 0.5, the deformed shape of cross section 'A', shown in Fig. 11a, indicates a small amount of outward deformation in the skin on each side of the stringer, and a small amount of twisting in the stringer deformation due to the asymmetry of the stringer Z cross section. For the case with the postbuckled skin and χ = -1.0, the deformed shape of cross section 'B' shows the skin deformed toward the stringer and bent over the stringer, with contact evident in the skin-stringer interface. At cross section 'C' of the postbuckled skin with χ = -1.0, the deformed shape shown in Fig. 11c shows the skin pulled away from the stringer, which causes the asymmetric stringer to twist. The skin and stringer separate on one side of the fastener row (see Fig. 11c), and the bending response of the skin is most severe in this region. There are significant bending stresses associated with the skin bending shown in Figs. 11b and 11c. The large stress values located in the skin-stringer attachment region will increase the likelihood of damage initiation and propagation in this region.
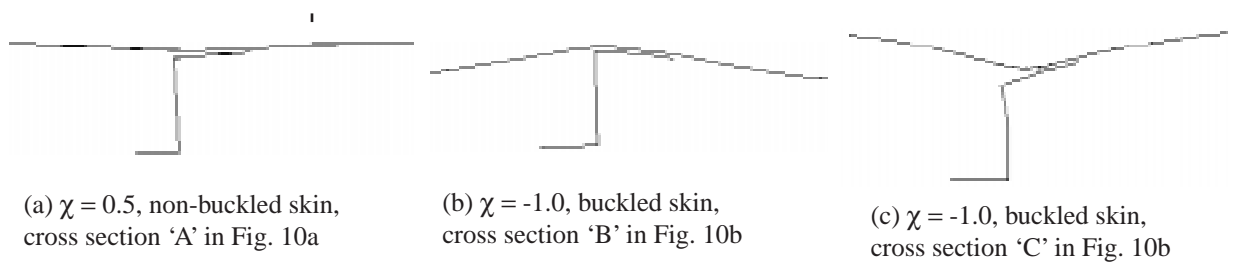

(a) χ = 0.5, non-buckled skin, cross section 'A' in Fig. 10a

(b) χ = -1.0, buckled skin, cross section 'B' in Fig. 10b

(c) χ = -1.0, buckled skin, cross section 'C' in Fig. 10b

Figure 11. Deformed shape (10x) of the stringer cross section for biaxial loading ratio values of χ = 0.5 and -1.0.

Centered 4-In.-Long Longitudinal Crack

The effects of cracks on the response was studied by modifying the finite element model to include a 4-in.-long longitudinal crack in the panel skin. The crack was located midway between frames, centered on x = 0 in Fig. 9, and adjacent to the line of skin-stringer attachment. Nonlinear analyses were conducted for an internal pressure load of 8 psi, and a range of axial load values corresponding to biaxial loading ratio values χ = 2.0 to -1.2. The 4-in.-long crack is large enough to influence the panel's overall response. Contour plots of the fuselage-skin radial displacement for biaxial loading ratio values χ = 0.5 and -1.0 are shown in Fig. 12. The displacement results indicate that the presence of the 4-in.-long crack influences the radial displacement in one skin bay on each side of the center stringer. The influence is not confined to the skin bay on the side of the stringer where the crack is located, because the crack unloads the circumferential tension load in the skin, and the stringer is not stiff enough in the circumferential direction to prevent the adjacent skin bay from also unloading.

For cases with all values of the biaxial loading ratio, the radial displacement is larger than in the pristine panel in the two skin bays adjacent to the crack, and the shape of the buckling deformation is different from the deformation in the remainder of the panel. The internal pressure causes outward bulging of the skin near the crack, and these bulging deformations are magnified when the panel is subjected to compressive loads. The deformations associated with the 4-in.-long crack dominate the local panel response and skin buckling deformation. The deformed shapes (3x magnification) of the center stringer near the 4-in.-long crack for biaxial loading ratio values of χ = 0.5 and -1.0 are shown in Fig. 13. The deformed shapes have significant displacements in the skin, but distortion of the stiffener cross-section appears to be minimal. The results of the analyses indicate that the stringer did not yield or collapse, and was able to support the additional loads developed by the crack.

The effects of combined loads and buckling deformations on fastener forces were also assessed. The maximum forces in the fasteners that connect the skin to the center stringer are reported in Table 1 for biaxial loading ratio values χ = 0.5 and -1.0. The maximum fastener loads are considerably larger than the values for the pristine panel. Compared to the pressure-only case, χ = 0.5, cases with pressure plus axial tension, χ > 0.5, have smaller fastener forces. When axial compression is applied and the skin buckles, as is the case for χ = -1.0, all of the fastener loads become significantly larger.
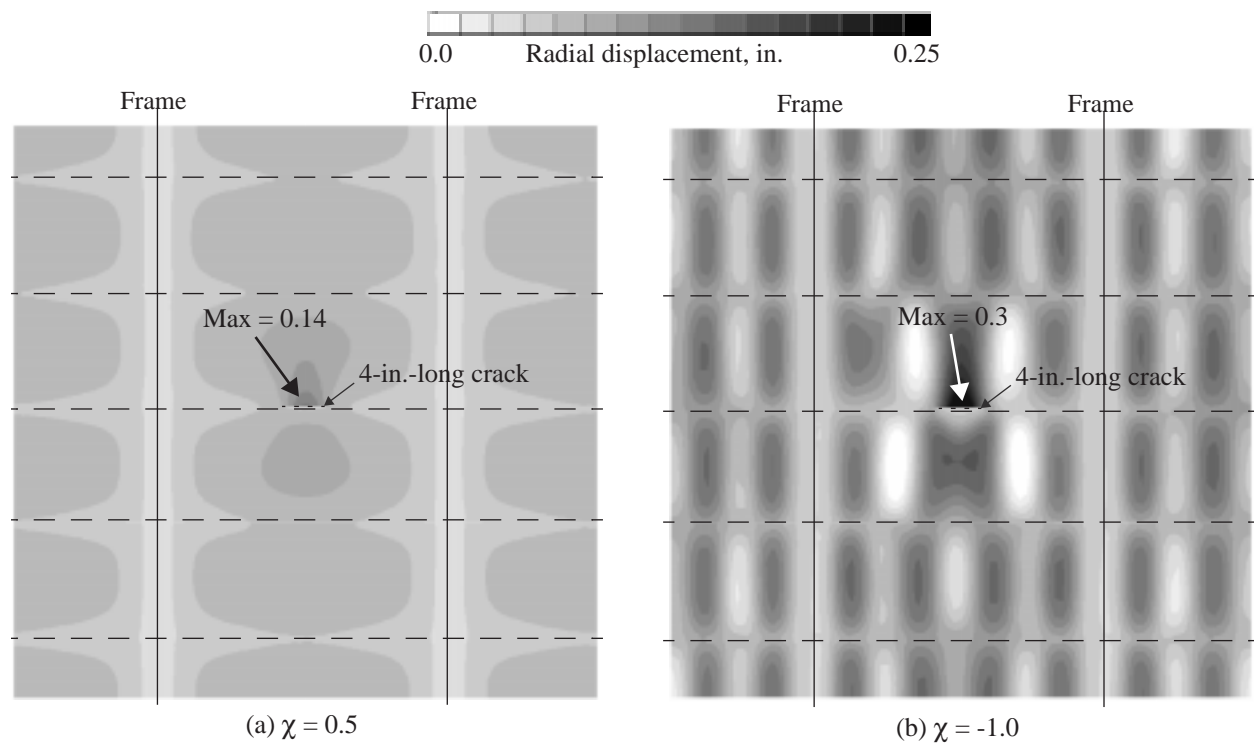

0.0   Radial displacement, in.   0.25

(a) χ = 0.5

(b) χ = -1.0

Figure 12. Radial displacement of fuselage-skin with a 4-in.-long longitudinal crack located midway between frames (x = 0.0) and adjacent to the center stringer, for biaxial loading ratio values of χ = 0.5 and -1.0
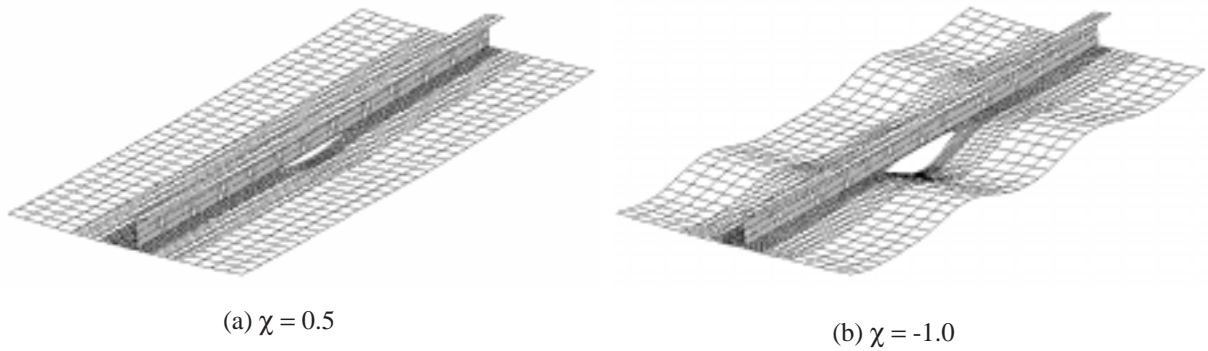
(a) χ = 0.5

(b) χ = -1.0

Figure 13. Deformed shape (3x) of the center stringer near a 4-in.-long crack for biaxial loading ratio values of χ = 0.5 and -1.0.

Table 1. Maximum fastener forces along the center stringer in a panel with a 4-in.-long longitudinal crack.

Biaxial loading ratio, χ	Tension, lb.	Axial shear, lb.	Side shear, lb.	Bending moment, in-lb.
0.5	18	58	55	3
-1.0	81	328	115	8

Stress intensity factors for the 4-in.-long longitudinal crack are shown in Fig. 14 for biaxial loading ratio values of χ = 2 to -1.2. In this figure, stress-intensity factors are normalized by the total stress intensity factor for the standard pressure-only condition. Results are shown for $\overline{K}_T$, the symmetric and asymmetric membrane components, $\overline{K}_I$ and $\overline{K}_{II}$, respectively, and the asymmetric bending component, $\overline{k}_2$. For the pressure-only case, χ = 0.5, and cases with pressure plus axial tension, χ > 0.5, the crack-tip response is dominated by $\overline{K}_I$, and the response is not very sensitive to

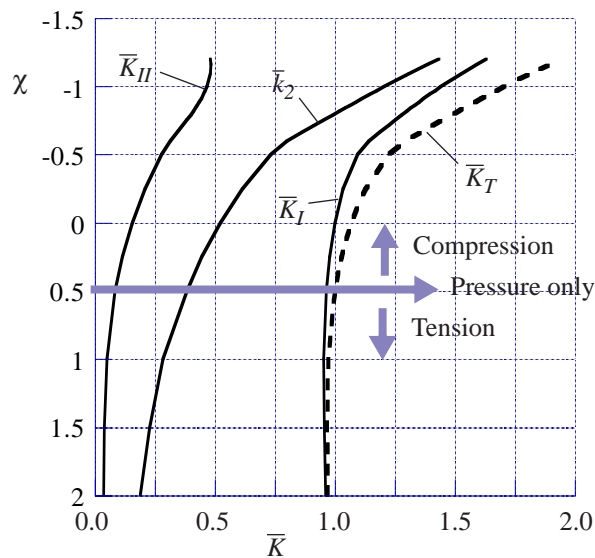**Figure 14. Stress intensity factors for a 4-in.-long longitudinal crack centered between frames (x = 0) and adjacent to the center stringer, for biaxial loading ratio values of χ = 2 to -1.2; normalized by $K_T = 36$ ksi√in. for χ = 0.5.**

variations in the biaxial loading ratio. When axial compression load is applied, $\chi < 0.5$, the stress intensity factors increase in magnitude in a manner that is typical of a limit-load response, rather than a bifurcation buckling response. That is, the bulging deformation near the crack develops gradually with increasing compression load, rather than changing suddenly when the skin buckles. For the maximum compression load considered, $\chi = -1.2$, $\overline{K}_I$ is 70% larger than $\overline{K}_I$ for the pressure-only case. Similarly, $\overline{k}_2$ and $\overline{K}_{II}$ are 270% and 460% larger, respectively, for $\chi = -1.2$, than their respective values for a pressure load only, $\chi = 0.5$. These elevated stress intensity factors can be related to accelerated crack growth rates and reduced residual strength.[27]

Summary Remarks

The results of this study indicate that nonlinear analyses of the stiffened-shell model can provide predictions of the geometric-nonlinear response of the buckled skin, cross section deformation of the stiffening components, and skin-stringer attachment forces associated with discrete fasteners. The numerical results indicate that compression loads and skin buckling can have a significant effect on the circumferential stress in the skin, and fastener loads, which will influence damage initiation. Compression loads and skin buckling have a comparable effect on stress intensity factors for cases with cracks, which will influence damage propagation rates and the residual strength of the panel.

V. Advances in Residual Strength Analyses from Laboratory Coupons to Structural Components

This section describes the residual strength analysis methodology developed at NASA Langley Research Center for aluminum aircraft fuselage structures with cracks and subjected to combined internal pressure and mechanical loads.[34] This methodology is applicable to complex built-up structure and accounts for combined loads, geometric nonlinearity, and material nonlinearity associated with elastic-plastic fracture. The methodology is based on the critical crack-tip-opening-angle (CTOA)[35-43] fracture criterion and the STAGS nonlinear finite element shell analysis code.[1] The critical CTOA criterion assumes that crack growth will occur when the local crack opening angle reaches a critical value. An elastic-plastic finite element analysis that allows cracks to propagate is needed to implement the criterion. The STAGS nonlinear shell analysis code has been developed to implement the criterion and to automatically extend a crack while the shell is in a nonlinear equilibrium state. The STAGS nonlinear shell analysis code is used with the critical CTOA criterion to perform the residual strength analyses for structures with geometric and material nonlinear behavioral characteristics.

Several studies have been conducted to confirm the use of the CTOA criterion in the STAGS analysis to predict the residual strength of a structure. The validation studies ranged in complexity from simple coupon tests, to unstiffened cylinder tests, up to complex built-up fuselage structure tests.[44-48] In the first validation effort, geometrically nonlinear elastic-plastic analyses were conducted to predict the response of compact-tension, C(T), and middle-crack-tension, M(T), panels, with and without buckling constraints. The experimental and predicted crack extension results for 2024-T3 C(T) and M(T) panels are shown in Fig. 15 as a function of the applied load. These results verify the selection of CTOA$_{cr}$ for this material and indicate that the analyses with STAGS accurately predict the reduction in strength of the panels caused by the geometrically nonlinear effect of panel buckling. Results for small-scale pressurized shells, flat stiffened panels, and curved stiffened panels were also obtained and are described below.

Pressurized Cylindrical Shell Tests

Unstiffened cylindrical shells were fabricated from 0.04-inch-thick 2024-T3 aluminum-alloy sheet, with the rolling direction orientated circumferentially. The shells were 39-inches long, 18 inches in diameter, and had a 1.5-inch-wide double lap splice with 0.04-inch-thick splice plates and a single row of rivets on each side of the splice. Each shell had a longitudinal crack that was simulated by a 0.01-inch-wide saw cut at the specimen mid-length, diametrically opposite to the lap-splice. Specimens with initial crack lengths of 2, 3, and 4 inches were loaded by internal pressure until failure occurred.[45] The crack length extension was recorded using crack wire gages.

The finite element models used to simulate the response of the cracked shells subjected to internal pressure took advantage of the symmetry of the problem and only a quarter of the shell was modeled. Self-similar crack growth (straight cracks) was assumed. The critical CTOA value used in the fracture analysis was the same as that used for the C(T) and M(T) panels of the same material and thickness.

The experimental measurements and the STAGS finite element predictions for the pressurized cylindrical shells with initial crack lengths of 2, 3, and 4 inches are shown in Fig. 16. The analyses predicted the maximum pressure to within 4% of the measured values, but tended to overpredict the pressure required to initiate crack growth. The use of saw cuts would generally cause the analysis to underpredict the pressure required to initiate the crack growth, since a
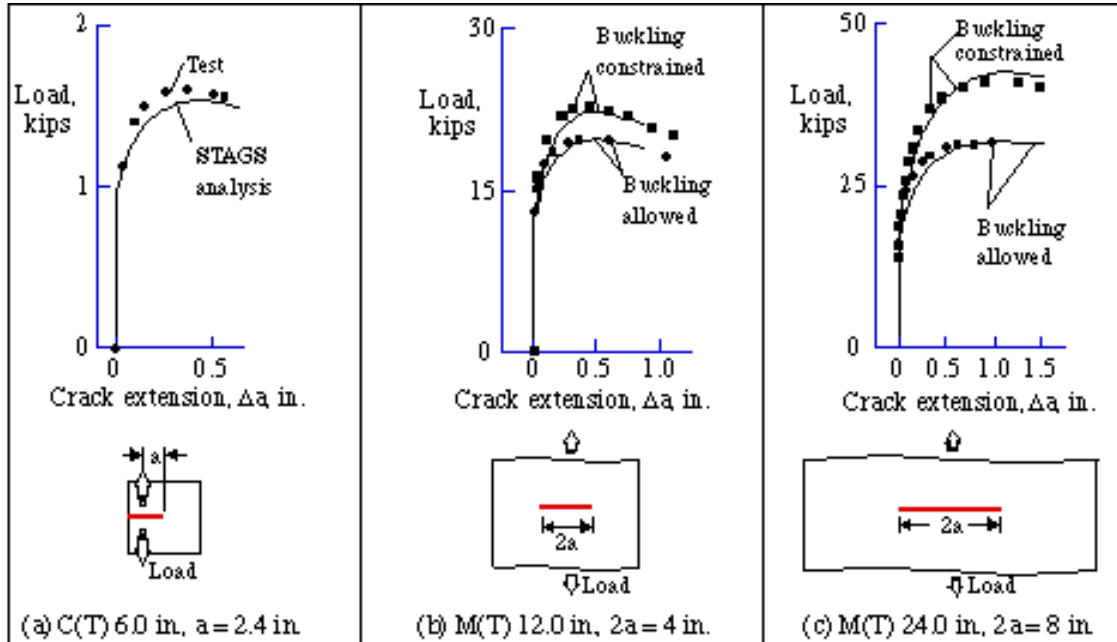
Figure 15.   Load versus crack extension results from C(T) and M(T) tests, and nonlinear STAGS analyses with CTOA$_{cr}$ = 5.0 deg. and hc = 0.04 in.

saw cut would require higher loads to initiate crack growth than a sharp fatigue crack.[49] One possible explanation for the overprediction of the pressure for initial crack growth could be that the intense crack-tip deformations might have caused the crack wire gages to register crack growth before the growth actually occurred.

Flat Stiffened Panel Tests

Fracture tests were conducted on 40-inch-wide, 0.063-inch-thick, 2024-T3 aluminum alloy, flat, stiffened panel specimens.[44] The stiffeners were made from 7075-T3 aluminum alloy and riveted to the specimens. The stiffeners were 1.6-inches wide and placed on both sides of the specimen, as illustrated in Fig. 17. The crack configuration of
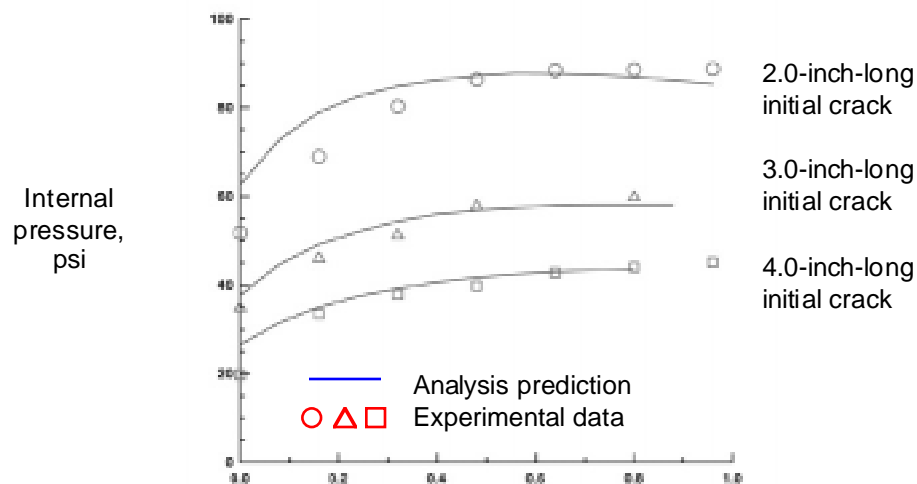

Figure 16. Comparison of analytical and experimental total crack extension results for 0.040-inch-thick internally pressurized shells.

the specimens consisted of a single 8-inch-long center crack with an array of twelve 3/16-inch-diameter holes on either side of the of the center crack. Specimens with and without MSD were tested. The MSD crack length was 0.05 inches from the edge of the hole. The specimens were tested without guide plates to allow out-of-plane displacements.

Predictions of the fracture behavior were conducted with the STAGS analysis code using a critical CTOA value obtained from smaller panel C(T) and M(T) tests. The configuration and loading condition were symmetric, so only a quarter of the sheet and stiffeners were modeled. The minimum element size along the line of crack extension was 0.04 inches. The analysis did not explicitly model the holes, but assumed that the holes with MSD cracks could be approximated with a crack with a length equal to the sum of the MSD crack lengths and the hole diameter. The rivet connections between the stiffener and sheet were modeled with nonlinear spring fastener elements with six degrees-of-freedom. A bifurcation buckling analysis was conducted to determine the first buckling mode shape, and this shape was introduced as an initial geometric imperfection with an amplitude of 10% of the panel thickness for the nonlinear analysis. To prevent element interpenetration, contact elements and multi-point constraint conditions were used to allow the panel sheet and stiffener surfaces to contact or separate during the response of the panel. The experimental measurements and finite element predictions for the stiffened panels with a single center crack are shown in Fig. 18. The results indicate that the analysis methodology represents the behavior of this specimen very well. Additional results in Ref. 44 indicate similar correlation was achieved for stiffened panels with MSD. The results from these tests and analyses confirm a residual strength prediction capability for flat stiffened panels with MSD.

Curved Stiffened Panel Tests

Three stringer- and frame-stiffened aluminum fuselage panels with longitudinal cracks were tested and analyzed at the NASA Langley Research Center using the analysis methodology described above.[46,47] These curved stiffened panels are referred to as Panels ASIP1, ASIP2, and ASIP3. Typical results are presented herein for Panels ASIP2 and ASIP3.

Panel ASIP2 has four stringers and three frames, and is shown prior to testing in Fig. 19a.[46] The overall dimensions of this panel include a 122-in. radius, a 72-in. length, and a 63-in. arc width. The skin is 0.063-in.-thick 2024-
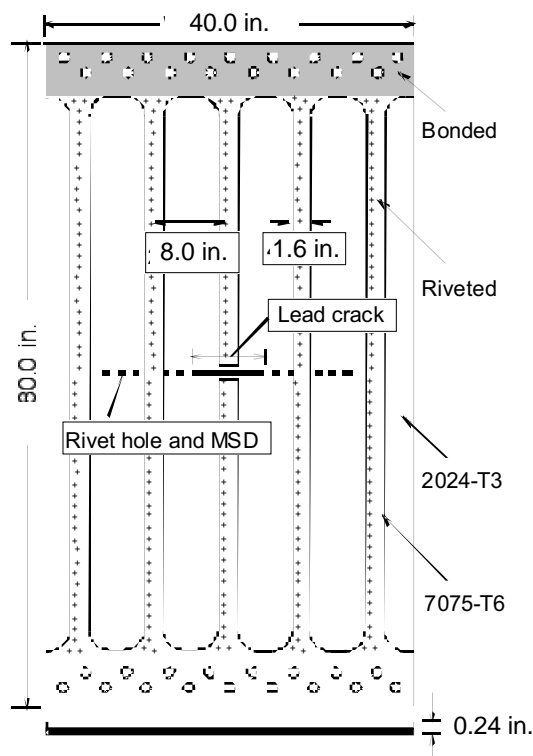

Figure 17. Wide stiffened flat panel and MSD configuration.
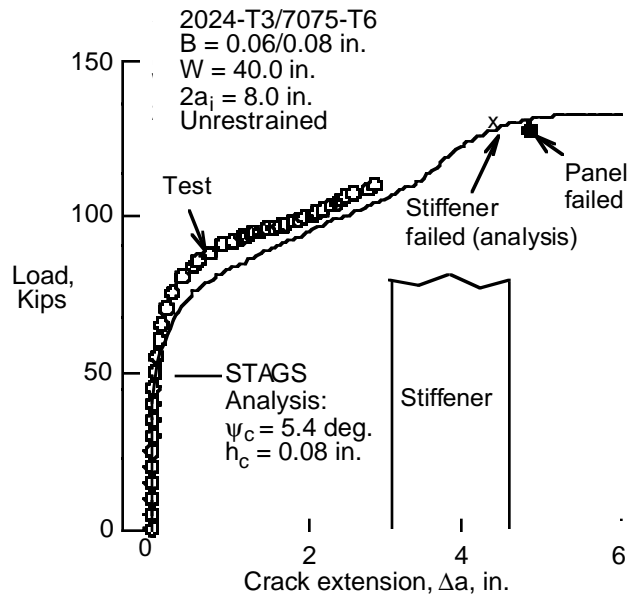
Figure 18. Experimental fracture measurements and STAGS finite element predictions for a 40-inch-wide, 2024-T3 aluminum alloy unrestrained stiffened panel with a single crack.

T3 aluminum alloy with the sheet rolling direction parallel to the stringers. The stringers are 2024-T3 aluminum-alloy inverted hat-section stringers with a stringer spacing of 14 in. The frames are 2024-T3 aluminum-alloy Z-section frames with a frame spacing of 22 in. There are 0.040-in.-thick 2024-T3 aluminum-alloy waffle tear straps, bonded to the skin, and located under the stringers and frames, but there are no tear straps midway between the frames. The stringers and frames are riveted to the skin and tear straps, and the frames are connected to the stringers by riveted stringer clips. Aluminum-alloy doublers are fastened to the curved ends of the panel between the stringers and along the sides of the panel between the frames to distribute the loads from the axial and circumferential or hoop load introduction plates of the test fixture into the panel skin. There is a lap joint in this panel under the second stringer from the left as the panel is shown in Fig. 19a. In the lap joint, the skin from the right side of the panel is the outer skin and overlaps at a greater radius over the inner skin from the left side of the panel. The layers of the lap joint are connected with three rows of 0.125-in.-diameter countersunk fasteners. The fastener pitch in the longitudinal direction is 1.0 in., and the three rows of fasteners are spaced 1.33 in. in the circumferential direction with the middle row of fasteners centered on a hat-section stringer. The initial damage for panel ASIP2 consisted of a 10-in.-long longitudinal lead crack and MSD cracks along the edge of the lap joint. The 10-in.-long lead crack was located adjacent to the second stringer and centered on a severed frame, as indicated in Fig. 19a. A schematic of the lap joint, shown in Fig. 19b, indicates that the lead crack was along the third row of fasteners in the lap joint. The MSD cracks were introduced prior to panel assembly by making small longitudinal cuts in the outer skin of the lap joint that extend 0.05 in. on each side of the fastener countersink for each fastener in the third row of fasteners. The resulting initial damage state was a 10-in.-long longitudinal lead crack with 0.33-in.-long MSD cracks in the outer skin, spaced ahead of the lead crack with a 1-in. pitch. The lead crack and MSD cracks were defined to be along the 'critical third row of fasteners' which is where lap joint eccentricity, pressure pillowing of the skin, and the fastener countersink combine to promote crack growth in the outer skin.

Panel ASIP3 has 12 stringers and five frames, and is shown prior to testing in Fig. 20. The overall dimensions of the panel include a 122-in. radius, a 120-in. length, and a 120-in. arc width. The initial damage for panel ASIP3 was a 10-in.-long longitudinal crack, located midway between stringers and centered on a severed frame, as indicated in
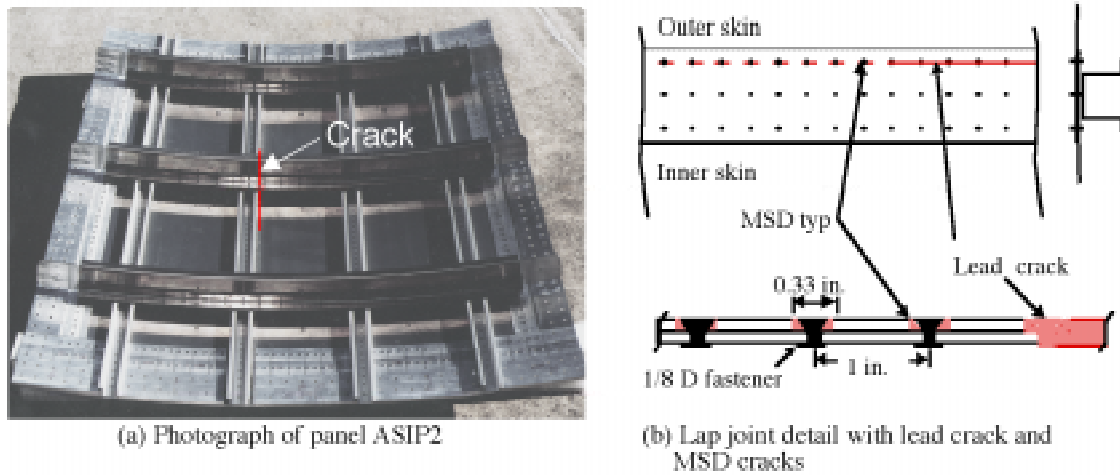
(a) Photograph of panel ASIP2

(b) Lap joint detail with lead crack and MSD cracks

Figure 19. Panel ASIP2 prior to testing.

Fig. 20. Details of panel ASIP3 are given in Ref. 47.

Panel ASIP2 was tested in a pressure-box test machine indicated in Fig. 21. The pressure-box test machine is capable of applying axial tensile loads of up to 7,000 lb/in. and internal pressure loads of up to 20 psi. Axial loads are applied at each end of the panel by two 225-kip hydraulic actuators connected to curved steel load introduction plates. Pressure is applied to the concave side of the panel using a 100-psi air supply source and a pneumatic control system. Circumferential or hoop loads that develop in the skin of the panel are reacted by flat steel load introduction plates attached to the straight edges of the panel, and two steel rods that connect each load introduction plate to the rigid steel frame of the pressure-box test machine. Circumferential or hoop loads that develop in the frames of the panel are re-acted by steel rods that connect each end of the panel frames to the rigid steel frame of the test machine. Each steel rod that reacts the circumferential loads includes a turnbuckle device that can be adjusted to ensure that circumferential loads of proper magnitudes are introduced in the panel frames and skin for a given loading condition. The reaction loads in the circumferential rods are measured by load cells built into the rods. A continuous rubber seal is connected to the bottom of the axial and circumferential load plates and to the top of the steel pressure containment box to permit the panel to float freely when pressurized and to minimize air leakage. The loading condition for panel ASIP2 was a combination of internal pressure plus axial tension loads. The axial load was prescribed to be equivalent to the bulk-
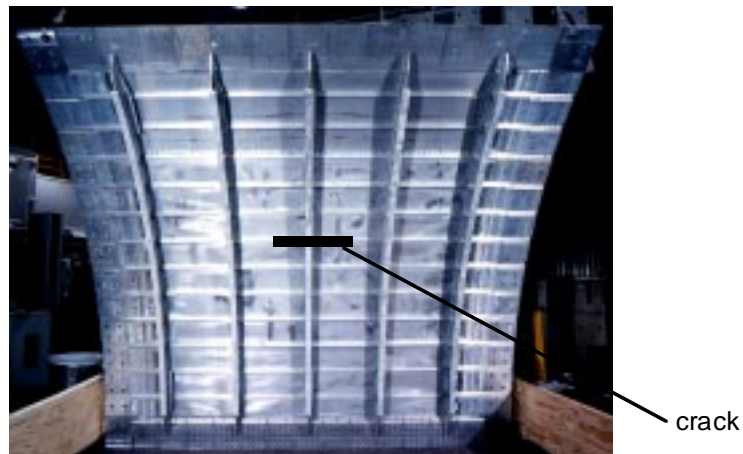

crack

Figure 20.   Panel ASIP3 prior to testing

head pressure load in a closed pressurized cylinder, and was applied during the test in proportion to the internal pressure load. Strain gages, linear variable displacement transducers, and video cameras were used to measure the panel response. Panel ASIP3 was tested in the COLTS combined loads test machine indicated in Fig. 22. The panel was attached to the D-box test fixture shown in the figure, and the panel was subjected to internal pressure, axial compression and torsion loads. Details of the test fixture for ASIP3 are given in Ref. 47.

The test results for panel ASIP2 indicate that the panel failed as a result of MSD crack link up. When panel ASIP2 was tested in the pressure-box test machine, the video record did not show any visible crack growth for pressure levels less than 9.95 psig. When the pressure reached 9.95 psig, the lead crack suddenly extended on each end of the crack, and linked up with the series of MSD cracks ahead of the lead crack. The crack extended in the longitudinal direction in a fast fracture mode, and extended over the entire panel length in an instant. The crack growth behavior was symmetric with respect to the central severed frame. Photographs which characterize the failure of panel ASIP2
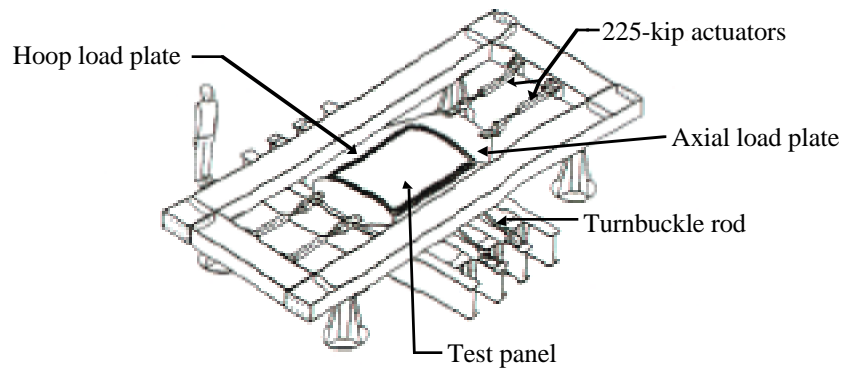

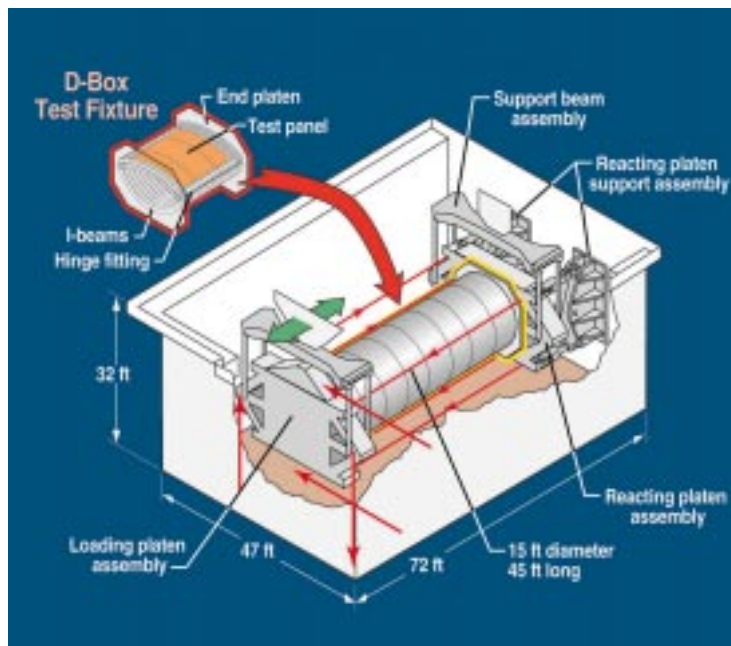**Figure 21. Pressure-box test machine.**
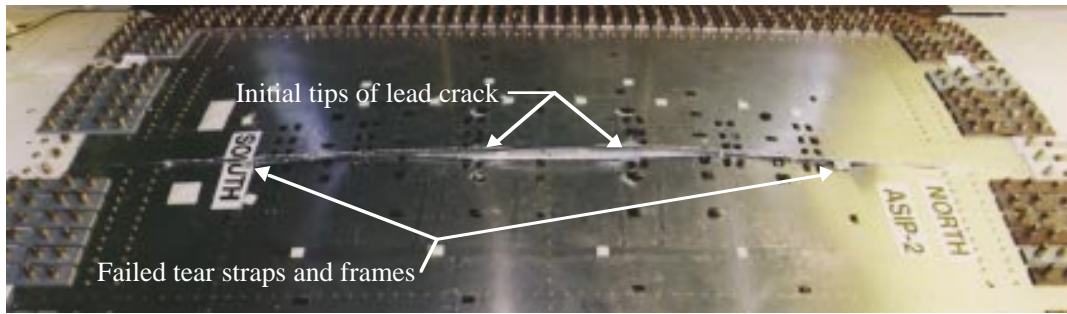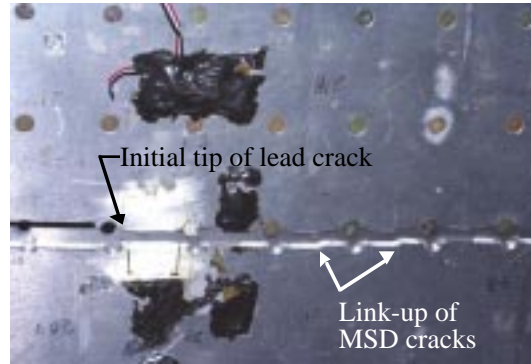

Figure 22. Combined loads test machine.

(a) Self-similar crack growth over the entire length of panel, failing adjacent tear straps and frames

(b) Failed tear strap and frame

(c) Crack trajectory with link-up of MSD cracks

Figure 23. Panel ASIP2 after testing.

(a) Hoop stress, σ_y
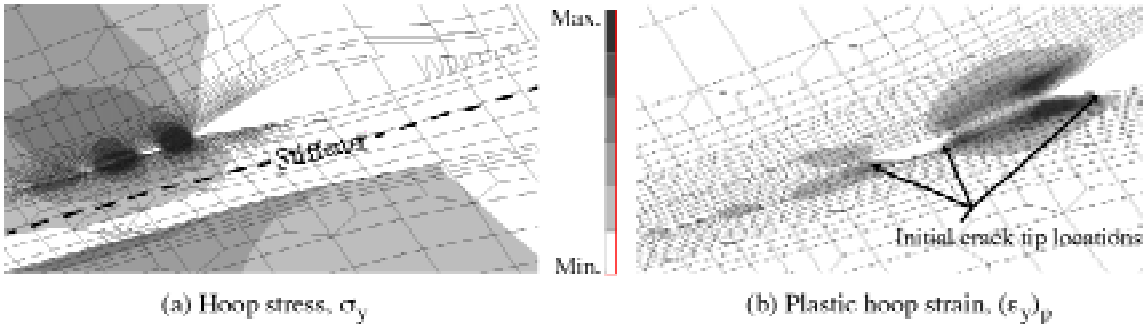

(b) Plastic hoop strain, $(\varepsilon_y)_p$

Figure 24. Typical analysis results for panel ASIP2 showing crack growth in the lead crack and MSD cracks.

are shown in Fig. 23. A view of the outer surface of the panel is shown in Fig. 23a, which shows that the skin crack has extended the full length of the panel. A view of the inner surface of the panel is shown in Fig. 23b which shows that the skin crack has extended past the adjacent frame and tear strap, failing each of these components at fastener hole locations. A close-up of the crack trajectory is shown in Fig. 23c which shows the link-up of the MSD cracks along the row of fasteners with the lead crack growing to the right, and the MSD cracks growing to the left and right so that link-up occurs midway between the fasteners. A typical solution with crack growth in the lead crack and the MSD cracks is shown in Fig. 24. The contour plot of the hoop stress in the region around the crack tip region, shown in Fig. 24a, indicates the high stress regions near the crack tips of the lead crack and the MSD cracks. A contour plot of the plastic strains in the hoop direction is shown in Fig. 24b which indicates that there are regions of plastic defor-

mation emanating from the lead crack and from the MSD crack tips, and that for the solution shown, the plastic zones from the lead crack and the first MSD crack have coalesced. The deformed shape shown in these plots indicates that the deformation on the side of the crack attached to the stiffener is much smaller than the deformation on the other side of the crack, demonstrating that the crack is not tearing due to a symmetric loading condition. The asymmetric loading could promote curvilinear crack growth, but it is assumed in the analysis that interaction between the lead crack and the MSD cracks will cause self-similar crack growth. The opening of the MSD cracks is also evident in the deformed shapes. The analysis predicted the residual strength of panel ASIP2 to within 11% of the experimentally observed value. For details on test and analysis correlation see Ref. 46.

The test results for panel ASIP3 indicate that the panel failed as a result of non-self-similar crack propagation. The loading condition for this panel included internal pressure, axial compression and torsion loads. The loading sequence for the panel consisted of applying the internal pressure load, followed by the axial compression load, and then followed by the torsion load. No crack growth was observed when the internal pressure and axial compression loads were applied. The torsion load was increased in magnitude until the crack propagated. A comparison of the analytically predicted crack growth trajectory and the test results for panel ASIP3 is shown in Fig. 25 indicating that the CTOA criterion and the nonlinear STAGS analysis predicted the crack growth trajectory very well for this combined loading condition. Details of the test and analysis results for panel ASIP3 are given in Ref. 47.

Summary Remarks

The results presented in this section demonstrate the fidelity of the residual strength analysis methodology developed at NASA Langley Research Center for aluminum aircraft fuselage structures with cracks and subjected to combined internal pressure and mechanical loads. The methodology is based on the critical crack-tip-opening-angle fracture criterion that characterizes the fracture behavior of a material of interest, and a geometric and material nonlinear finite element shell analysis code that performs the structural analysis of a fuselage structure of interest. The results indicate that elastic-plastic effects in a thin sheet can be effectively represented by a critical-crack-tip-opening-angle fracture criterion. The results also indicate that geometric and material nonlinear structural analyses can accurately represent the changes in internal load distributions, local stress and displacement gradients, and crack growth behavior in stiffened fuselage shells that are subjected to combined internal pressure and mechanical loads and have long cracks. In addition, nonlinear fracture analysis and structural analysis methods provide higher fidelity results than traditional linear-elastic engineering analysis approximations for structures with significant plastic yielding and nonlinear out-of-plane deformations associated with internal pressure loads. Numerical models and structural analysis methods must accurately represent the multiple length scales associated with simulating the global response of a large stiffened shell structure, the local deformations, and the internal load redistribution as damage propagates in the structure.

The results presented in this section represent what is currently possible with a state-of-the-art residual strength analysis methodology. This analysis methodology is possible today because verified high-fidelity nonlinear structural
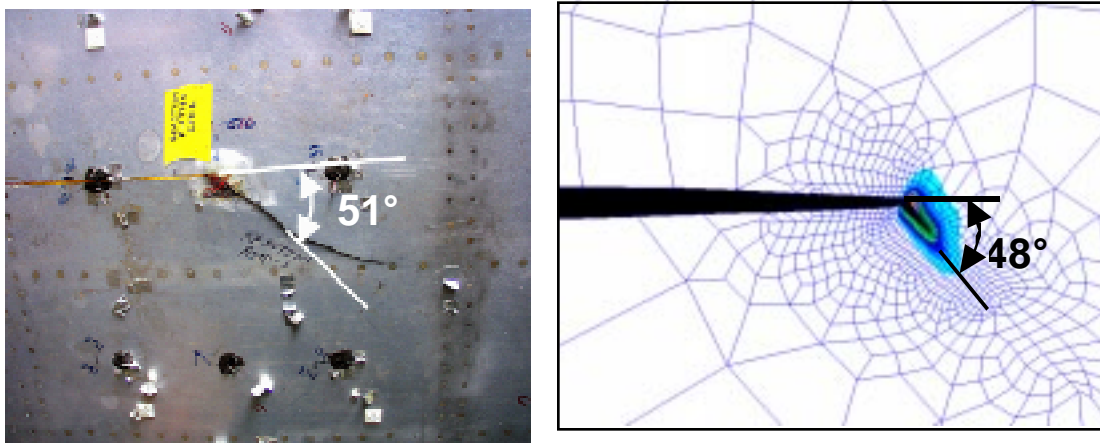
(a) Experimental results.

(b) Analytical results.

Figure 25.   Panel ASIP3 crack growth trajectory.

analysis tools are emerging; high-capacity computing engines are becoming affordable; insight into the complex structural response and failure characteristics of structures subjected to combined loads is developing; physics-based failure initiation and propagation analyses are emerging; and the underlying scientific basis for high-fidelity analysis and design technology is emerging.

VI. Concluding Remarks

Results from research efforts in residual strength analysis of metallic fuselage structures have been presented. These efforts were led by Jim Starnes and were the product of his vision for solving this complex problem. Jim's major contributions to advances in residual strength analysis methods for metallic structes were in identifying the effect of combined internal pressure and mechanical loads and geometric nonlinearity on the response of built-up structure with damage. Through Jim's leadership, research was conducted that demonstrated that the linear pressure-only case often used by industry may be unconservative in some cases, and over-conservative in other cases.

In addition, a residual strength analysis methodology for fuselage structure with cracks has been developed and verified by experiments. Fifteen years ago, the aircraft industry would not consider using nonlinear analysis for structures with cracks. Today, personal communications indicate that the verified analysis methodology and analysis code described in this paper have been used by the aircraft industry to realize improved analyses and design capability. A few examples include Boeing's use of nonlinear parametric analyses to update their damage tolerance design guide for stiffened panels, and using nonlinear residual strength analyses to predict the strength of a DC-9 aft bulkhead and KC-135 fuselage panels. In addition, Lockheed Marietta has used this analysis methodology to improve life predictions and refine inspection schedules for Strategic Airlift Aircraft (C-5). The residual strength analysis methodology is currently being incorporated into the ABAQUS commercial finite element code. The CTOA fracture criterion has already been implemented in the ABAQUS code and efforts are underway to adopt residual strength solution algorithms from STAGS for use in ABAQUS.

In 1999, NASA recognized this research with a "Turning Goals into Reality" Award for valuable contributions to the NASA Airframe Structural Integrity Team and exceptional progress toward aviation safety. The success of this research can be largely attributed to the technical guidance and vision that Jim Starnes provided for the research team. The research effort spanned several years, involved many complex phenomena, and required contributions from several disciplines and many researchers. Through Jim's vision, he was able to address the complex research problem through a series of smaller problems, and then integrate the research findings into a general capability for solving real-world fuselage problems.

Jim's contributions to this research activity, and to the many other research activities he led, go well beyond the technical results that were generated. His knowledge and his vision provided direction, sometimes direction not fully appreciated, and while assembling this paper it was realized that our understanding of Jim's vision continues to grow. His never ending enthusiasm kept us going and striving to learn more. Perhaps teaching of his research approach was his largest contribution as we now apply his approach to guide us in our research.

VII. References

[1]Rankin, C. C., Brogan, F. A., Loden, W. A. and Cabiness, H. D., "STAGS User Manual, Version, 5.0," Lockheed Martin Missiles & Space Co., Inc., Rept. LMSC P032594, January 2005.

[2]Swift, T., "Damage Tolerance in Pressurized Fuselages," *New Materials and Fatigue Resistant Aircraft Design*, D. L. Simpson, Ed., EMAS Ltd., 1987, pp.1-77.

[3]Starnes, J. H., Jr., Britt, Vicki O., and Rankin, C. C., "Nonlinear Response of Damaged Stiffened Shells Subjected to Combined Internal Pressure and Mechanical Loads," AIAA Paper 95-1462, April 1995.

[4]Starnes, J. H., Jr., Britt, V. O., Rose, C. A., and Rankin, C. C., "Nonlinear Response and Residual strength of Damaged Stiffened Panels Subjected to Combined Loads," AIAA Paper No. 96-1555, April 1996.

[5]Starnes, J. H., Jr., Rose, C. A., Young, R. D., and Rankin, C. C., "Effects of Combined Loads on the Nonlinear Response of Stiffened Shells with Long Cracks," Presented at the 19th International Committee on Aeronautical Fatigue Symposium, Edinburgh, Scotland, UK, June 18-20, 1997

[6]Young, R. D., Rose, C. A., and Starnes, J. H., Jr., "Nonlinear Bulging Factors for Longitudinal and Circumferential Cracks in Cylindrical Shells Subjected to Combined Loads," Proceedings of the 41st AIAA/ASME/ASCE/AHS/ASC Structures, Structural Dynamics and Materials Conference, Atlanta, GA, April 2000, AIAA Paper No. 2000-1514.

[7]Folias, E. S., "An Axial Crack in a Pressurized Cylindrical Shell," *International Journal of Fracture Mechanics,* Vol. 1, No. 2, 1965, pp. 104-113.

[8]Folias, E. S., "A Circumferential Crack in a Pressurized Cylindrical Shell," *International Journal of Fracture Mechanics,* Vol. 3, 1967, pp. 1-12.

[9]Folias, E. S., "On the Effect of Initial Curvature on Cracked Flat Sheets," *International Journal of Fracture Mechanics,* Vol. 5, No. 4, December 1969, pp. 327-346.

[10]Folias, E. S., "Asymptotic Approximations to Crack Problems in Shells," *Mechanics of Fracture - Plates and Shells with Cracks,* G. C. Sih, H. C. van Elst, and D. Broek, eds., Noordhoff International, Leyden, 1977, pp. 117-160.

[11]Copely, L. G., and Sanders, J. L., Jr., "A Longitudinal Crack in a Cylindrical Shell under Internal Pressure," *International Journal of Fracture Mechanics,* Vol. 5, No. 2, June 1969, pp. 117-131.

[12]Erdogan, F., and Kibler, J. J., "Cylindrical and Spherical Shells with Cracks," *International Journal of Fracture Mechanics,* Vol. 5, No. 3, September 1969, pp. 229-237.

[13]Erdogan, F., and Ratwani, M., "Fatigue and Fracture of Cylindrical Shells Containing a Circumferential Crack," *International Journal of Fracture Mechanics,* Vol. 6, No. 4, September 1970, pp. 379-392.

[14]Duncan-Fama, M. E., and Sanders, J. L., Jr., "A Circumferential Crack in a Cylindrical Shell under Tension," *International Journal of Fracture Mechanics*, Vol. 8, No. 1, March 1972, pp. 15-20.

[15]Peters, Roger W., and Kuhn, Paul, "Bursting Strength of Unstiffened Pressure Cylinders with Slits," NACA TN 3993, April 1957.

[16]Anderson, Robert B., and Sullivan, Timothy L., "Fracture Mechanics of Through-Cracked Cylindrical Pressure Vessels," NASA TN D-3252, February 1966.

[17]Chen, D., "Bulging of Fatigue Cracks in a Pressurized Aircraft Fuselage," Ph.D. Thesis, Delft University of Technology, Delft, The Netherlands, Report LR-647, October 1990.

[18]Jeong, D. Y., and Tong, P., "Nonlinear Bulging Factor Based on R-Curve Data," Proceedings of the FAA/NASA International Symposium on Advanced Structural Integrity Methods for Airframe Durability and Damage Tolerance, September 1994, pp. 327-338.

[19]Bakuckas, J. G., Ngugen, P. V., and Bigelow, C. A., "Engineering Fracture Parameters for Bulging Cracks in Pressurized Unstiffened Curved Panels," Proceedings of the FAA-NASA Symposium on Continued Airworthiness of Aircraft Structures, DOD/FAA/AR-97/2, 1996.

[20]Bakuckas, J. G., Jr., Nguyen, P. V., Bigelow, C. A., and Broek, D., "Bulging Factors for Predicting Residual Strength of Fuselage Panels," Presented at the International Conference on Aeronautical Fatigue, Edinburgh, Scotland, June 18-20, 1997.

[21]Riks, E., "Bulging Cracks in Pressurized Fuselages: A Numerical Study," NLR Report NLR-MP-87058 U, NLR National Aerospace Laboratory, The Netherlands, 1978.

[22]Riks, E., Brogan, F. A., and Rankin, C. C., "Bulging Cracks in Pressurized Fuselages: A Procedure for Computation," in Analytical and Computational Models of Shells, Noor, A. K., Belytschko, T., and Simo, J. C., eds., The American Society of Mechanical Engineers, ASME-CED, Vol. 3, 1989.

[23]Budiman, H. T., and Lagace, P. A., "Nondimensional Parameters for Geometric Nonlinear Effects in Pressurized Cylinders with Axial Cracks," *Journal of Applied Mechanics*, Vol. 64, 1997, pp. 401-407.

[24]Budiman, H. T., "Mechanisms of Damage Tolerance and Arrest in Pressurized Composite Cylinders," Ph.D. Thesis, Department of Aeronautics and Astronautics, Massachusetts Institute of Technology, Cambridge, MA, 1996.

[25]Young, R. D., Rose, C. A., and Starnes, J. H., Jr., "Nonlinear Local Bending Response and Bulging Factors for Longitudinal and Circumferential Cracks in Pressurized Shells," Proceedings of the 3rd Joint FAA/DoD/NASA Conference on Aging Aircraft, Albuquerque, NM, September 20-23, 1999.

[26]Rose, C. A., Young, R. D., and Starnes, J. H., Jr., "Nonlinear Local Bending Response and Bulging Factors for Longitudinal Cracks in Pressurized Cylindrical Shells," Proceedings of the 40th AIAA/ASME/ASCE/AHS/ASC Structures, Structural Dynamics, and Materials Conference, St. Louis, MO, April 12-15, 1999, AIAA Paper No. 99-1412.

[27]Young, R. D., Rose, C. A., and Starnes, J. H., Jr., "Skin, Stringer, and Fastener Loads in Buckled Fuselage Panels," Proceedings of the 42st AIAA/ASME/ASCE/AHS/ASC Structures, Structural Dynamics and Materials Conference, Seattle, WA, April 2001, AIAA Paper No. 2001-1326.

[28]Rose, C. A., Young, R. D., and Starnes, J. H., Jr., "The Nonlinear Response of Cracked Aluminum Shells Subjected to Combined Loads," Proceedings of the 42nd AIAA/ASME/ASCE/AHS/ASC Structures, Structural Dynamics and Materials Conference, Seattle, WA, April 2001, AIAA Paper No. 2001-1395.

[29]Starnes, J. H., Jr., and Rose, C. A., "Nonlinear Response of Thin Cylindrical Shells with Longitudinal Cracks and Subjected to Internal Pressure and Axial Compression Loads," Proceedings of the 38th AIA/ASME/ASCE/AHS/ASC Structures, Structural Dynamics and Materials Conference, April 1997, AIAA Paper No. 97-1144, April 1997.

[30]Ratwani, M. M., and Wilhem, D. P., "Influence of Biaxial Loading on Analysis of Cracked Stiffened Panels," Engineering Fracture Mechanics, Vol. 11, 1979, pp. 585-593.

[31]Gökgöl, O., "Crack Free and Cracked Life of the Pressurized Cabin of the A300B – Calculation, Tests and Design Measurements to Improve Damage Tolerance," Aeronautical Journal, January 1979.

[32]Rybicki, E. F., and Kanninen, M. F., "A Finite Element Calculation of Stress Intensity Factors by a Modified Crack Closure Integral," Engineering Fracture Mechanics, Vol. 9, 1977, pp. 931-938.

[33]Hui, C. Y., and Zehnder, A. T., "A Theory for the Fracture of Thin Plates Subjected to Bending and Twisting Moments," International Journal of Fracture, Vol. 61, No. 3, 1993, pp. 211-229.

[34]Starnes, J. H., Jr., Newman, J. C., Jr., Harris, C. E., Young, R. D., Rose, C. A., and James, M. A., "Advances in Residual Strength Analyses from Laboratory Coupons to Structural Components," Proceedings of the ICAF 2001 International Committee on Aeronautical Fatigue 21st Symposium, Toulouse, France, June 2001.

[35]Newman, J.C., Jr., "An Elastic-Plastic Finite Element Analysis of Crack Initiation, Stable Crack Growth, and Instability," ASTM STP 833, 1984, pp. 93-117.

[36]Dawicke, D. S., Sutton, M. A., Newman, J. C., Jr., and Bigelow, C. A., "Measurement and Analysis of Critical CTOA for an Aluminum Alloy Sheet," NASA TM-109024, September 1993.

[37]Dawicke, D. S. and Newman, J. C., Jr., "Residual Strength Predictions for Multiple Site Damage Cracking Using a Three-Dimensional Finite Element Analysis and a CTOA Criterion," In Fatigue and Fracture Mechanics: 29th Volume, ASTM STP 1332, 1998, pp. 815-829.

[38]Dawicke, D. S. and Sutton, M. A., "Crack Tip Opening Angle Measurements and Crack Tunneling Under Stable Tearing in Thin Sheet 2024-T3 Aluminum Alloy," NASA CR-191523, September 1993.

[39]Shivakumar, K. N. and Newman, J. C., Jr., "ZIP3D - An Elastic-Plastic Finite-Element Analysis Program for Cracked Bodies," NASA TM-102753, 1990.

[40]Dawicke, D. S. and Newman, J. C., Jr., "Residual Strength Predictions for Multiple Site Damage Cracking Using a Three-Dimensional Finite Element Analysis and a CTOA Criterion," In Fatigue and Fracture Mechanics: 29th Volume, ASTM STP 1332, T. L. Panontin and S. D. Sheppard, Eds. American Society for Testing and Materials, 1998.

[41]Dawicke, D. S., Newman, J.C., Jr., and Bigelow, C. A., "Three-Dimensional CTOA and Constraint Effects During Stable Tearing in a Thin-Sheet Material," In Fracture Mechanics: 26th Volume, ASTM STP 1256, 1995, pp. 223-242.

[42]Newman, J. C., Jr., "Finite Element Analyses of Fatigue Crack Propagation -- Including the Effects of Crack Closure," Ph.D. Thesis, Virginia Polytechnic institute and State University, Blacksburg, VA, May 1974.

[43]Dawicke, D. S., "Residual Strength Predictions Using a Crack Tip Opening Angle Criterion," FAA-NASA Symposium on the Continued Airworthiness of Aircraft Structures, DOT/FAA/AR-97/2, Vol. II, July 1997, pp. 555-566.

[44]Seshadri, B. R., Newman, J. C., Jr., Dawicke, D. S., and Young, R. D., "Fracture Analysis of the FAA/NASA Wide Stiffened Panels," Proceedings of the FAA-NASA Symposium on the Continued Airworthiness of Aircraft Structures," DOT/FAA/AR-92/2, 1997, pp. 513-524.

[45]Starnes, James H., Jr., and Rose, Cheryl A., "Stable Tearing and Buckling Response of Unstiffened Aluminum Shells with Long Cracks." Proceedings of the Second Joint NASA/FAA/DOD Conference on Aging Aircraft, Williamsburg, VA, August 31-September 3, 1998. NASA/CP-1999-208982/Part 1, pp. 610-626, January 1999.

[46]Young, Richard D., Rouse, Marshall, Ambur, Damodar R., and Starnes, James H., Jr., "Residual Strength Pressure Tests and Nonlinear Analyses of Stringer- and Frame-Stiffened Aluminum Fuselage Panels with Longitudinal Cracks," Proceedings of the Second Joint NASA/FAA/DOD Conference on Aging Aircraft, Williamsburg, VA, August 31-September 3, 1998. NASA/CP-1999-208982/Part 1, pp. 408-426, January 1999.

[47]Ambur, Damodar R., Rouse, Marshall, Young, Richard D., and Perez-Ramos, Carlos, "Evaluation of an Aluminum Panel with Discrete-Source Damage and Subjected to Combined Loading Conditions," Proceedings or the 40th AIAA/ ASME/ASCE/AHS/ASC Structures, Structural Dynamics, and Materials Conference, St. Louis, MO, April 12-15, 1999. AIAA Paper AIAA-99-1439, 1999.

[48]Dawicke, David S., Newman, James C., Jr., Starnes, James H., Jr., Rose, Cheryl A.; Young, Richard D. and Seshadri, B. R., "Residual Strength Analysis Methodology: Laboratory Coupons to Structural Components," Proceedings of the Third Joint FAA/DOD/NASA Conference on Aging Aircraft, Albuquerque, NM, September 20-23, 1999.

[49]Dawicke, D. S., Newman, J. C., Jr., Sutton, M. A., and Amstutz, B. E., "Influence of Crack History on the Stable Tearing Behavior of a Thin-Sheet Material with Multiple Cracks," NASA CP 3274, FAA/NASA International Symposium on Advanced Structural Integrity Methods for Airframe Durability and Damage Tolerance, Part 1, 1994, pp. 193-212.